

Models of the Structure and Evolution of Protoplanetary Disks

C.P. Dullemond

Max-Planck-Institute for Astronomy, Heidelberg

D. Hollenbach

NASA-Ames Research Center

I. Kamp

Space Telescope Division of ESA

P. D'Alessio

Centro de Radioastronomía y Astrofísica, UNAM, México

We review advances in the modeling of protoplanetary disks. This review will focus on the regions of the disk beyond the dust sublimation radius, i.e. beyond 0.1 - 1 AU, depending on the stellar luminosity. We will be mostly concerned with models that aim to fit spectra of the dust continuum or gas lines, and derive physical parameters from these fits. For optically thick disks, these parameters include the accretion rate through the disk onto the star, the geometry of the disk, the dust properties, the surface chemistry and the thermal balance of the gas. For the latter we are mostly concerned with the upper layers of the disk, where the gas and dust temperature decouple and a photoevaporative flow may originate. We also briefly discuss optically thin disks, focusing mainly on the gas, not the dust. The evolution of these disks is dominated by accretion, viscous spreading, photoevaporation, and dust settling and coagulation. The density and temperature structure arising from the surface layer models provide input to models of photoevaporation, which occurs largely in the outer disk. We discuss the consequences of photoevaporation on disk evolution and planet formation.

1. INTRODUCTION

Dusty circumstellar disks have been the focus of intense observational interest in recent years, largely because they are thought to be the birthplaces of planetary systems. These observational efforts have yielded many new insights on the structure and evolution of these disks. In spite of major developments in spatially resolved observations of these disks, much of our knowledge of their structure is still derived from spatially *unresolved* spectroscopy and spectral energy distributions (SEDs). The interpretation of this information (as well as spatially resolved data) requires the use of theoretical models, preferentially with as much realism and self-consistency as possible. Such disk models have been developed and improved over many years. When they are in reasonable agreement with observations they can also serve as a background onto which other processes are modeled, such as chemistry, grain growth, and ultimately the formation of planets.

This chapter reviews the development of such self-consistent disk structure models, and discusses the current status of the field. We focus on the regions of the disk beyond the dust sublimation radius, since the very inner regions are discussed in the chapter by Najita et al.. To limit our scope further, we restrict our review to models primarily aimed at a comparison with observations. We

will start with a concise resumé of the formation and viscous evolution of disks (Section 2). This sets the radial disk structure as a function of time. We then turn our attention to the vertical structure, under the simplifying assumption that the gas temperature equals the dust temperature everywhere (Section 3). While this assumption is valid in the main body of the disk, it breaks down in the disk surface layers. Section 4 treats the gas physics and chemistry of these surface layers, where much of the spectra originate. Photoevaporation flows also originate from the warm surface layers, and affect the disk evolution, which is the topic of Section 5.

2. FORMATION AND VISCOUS EVOLUTION OF DISKS

The formation of stars and planetary systems starts with the gravitational collapse of a dense molecular cloud core. Since such a core will always have some angular momentum at the onset of collapse, most of the infalling matter will not fall directly onto the protostar, but form a disk around it (e.g., *Terebey et al.*, 1984; *Yorke et al.*, 1993) or fragment into a multiple stellar system (e.g., *Matsumoto and Hanawa*, 2003). Because of the complexity of the latter, we focus on the single star formation scenario here. While matter falls onto the disk, viscous stresses and grav-

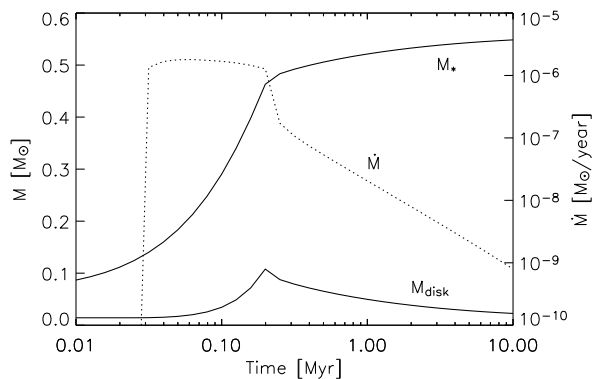


Fig. 1.— Evolution of various disk and star quantities as a function of time after the onset of collapse of the cloud core (after *Hueso and Guillot, 2005*). Solid lines: stellar mass (upper) and disk mass (lower). Dotted line: accretion rate *in the disk*. In this model the disk is formed at $t \simeq 0.03$ Myr, causing the jump in the dotted line at this point. The collapse phase is finished by 2×10^5 years.

itational torques within the disk will transport angular momentum to its outer regions. As a consequence of this, most of the disk matter moves inward, adding matter to the protostar, while some disk matter moves outward, absorbing all the angular momentum (*Lynden-Bell and Pringle, 1974*). During its formation and evolution a disk will spread out to several 100 AU or more (*Nakamoto and Nakagawa, 1994*, henceforth NN94; *Hueso and Guillot, 2005*, henceforth HG05). This spreading is only stopped when processes such as photoevaporation (this chapter), stellar encounters (*Scally and Clarke, 2001; Pfalzner et al., 2005*) or a binary companion (*Artymowicz and Lubow, 1994*) truncate the disk from the outside. During the collapse phase, which lasts a few $\times 10^5$ years, the accretion rate within the disk is very high ($\dot{M} \sim 10^{-5} - 10^{-6} M_{\odot}/\text{yr}$), but quickly drops to $\dot{M} \sim 10^{-7} - 10^{-9} M_{\odot}/\text{yr}$ once the infall phase is over (NN94, HG05). The optical and ultraviolet excess observed from classical T Tauri stars (CTTSs) and Herbig Ae/Be stars (HAeBes) confirms that this on-going accretion indeed takes place (*Calvet et al., 2000*, and references therein). In Fig. 1 we show the evolution of various disk and star parameters.

2.1. Anomalous viscosity

An issue that is still a matter of debate is what constitutes the viscosity required for disk accretion, particularly after infall has ceased. Molecular viscosity is too small to account for the observed mass accretion rates. Turbulent and magnetic stresses, however, can constitute some kind of anomalous viscosity. The magnetorotational instability (MRI), present in weakly magnetized disks, is the most accepted mechanism to drive turbulence in disks and transport angular momentum outwards (*Balbus and Hawley, 1991; Stone and Pringle, 2001; Wardle, 2004*, and ref-

erences therein).

There is a disk region ($0.2 < r < 4$ AU, for typical CTTS disk parameters according to *D’Alessio et al., 1998*) in which the ionization fraction is smaller than the minimum value required for the MRI. Neither thermal ionization (requiring a temperature higher than 1000 K), cosmic ray ionization (requiring a mass surface density smaller than $\sim 100 \text{ g/cm}^2$) (*Jin, 1996; Gammie, 1996*), nor X-rays (*Glassgold et al., 1997a, 1997b*) are able to provide a sufficient number of free electrons to have MRI operating near the midplane. *Gammie (1996)* proposed a layered accretion disk model, in which a “dead zone” is encased between two actively accreting layers. The precise extent of this dead zone is difficult to assess, because the number density of free electrons depends on detailed chemistry as well as the dust grain size distribution, since dust grains tend to capture free electrons (*Sano et al., 2000*, and references therein). If the disk dust is like the interstellar dust, the MRI should be inhibited in large parts of the disk (*Ilgner and Nelson, 2006*), though this is still under debate (e.g. *Semenov et al., 2004*; see chapter by *Bergin et al.*).

There are also other (non-magnetic) mechanisms for anomalous viscosity, like the baroclinic instability (*Klahr and Bodenheimer, 2003*) or the shear instability (*Dubrulle et al., 2005*), which are still subject to some controversy (see the recent review by *Gammie and Johnson, 2005*). Angular momentum can also be transferred by global torques, such as through gravitational spiral waves (*Tohline and Hachisu, 1990; Laughlin and Bodenheimer, 1994; Pickett et al., 2003* and references therein) or via global magnetic fields threading the disk (*Stehle and Spruit, 2001*), possibly with hydromagnetic winds launched along them (*Blandford and Payne, 1982; Reyes-Ruiz and Stepinski, 1996*).

2.2. α -Disk models for protoplanetary disks

To avoid having to solve the problem of viscosity in detail, but still be able to produce sensible disk models, *Shakura and Sunyaev (1973)* introduced the “ α -prescription”, based on dimensional arguments. In this recipe the vertically averaged viscosity ν at radius r is written as $\nu = \alpha H_p c_s$, where H_p is the pressure scale height of the disk and c_s is the isothermal sound speed, both evaluated at the disk midplane where most of the mass is concentrated. The parameter α summarizes the uncertainties related to the sources of anomalous viscosity, and is often taken to be of the order of $\alpha \simeq 10^{-2}$ for sufficiently ionized disks.

From conservation of angular momentum, the mass surface density Σ of a *steady* disk (i.e. with a constant mass accretion rate \dot{M}), for radii much larger than the disk inner radius r_{in} , can be written as $\Sigma(r) \approx \dot{M}/3\pi\nu$. With $H_p = c_s/\Omega_K$, where Ω_K is the Keplerian angular velocity, we see that for $r \gg r_{\text{in}}$,

$$\Sigma(r) = K \frac{\dot{M}}{r^{3/2} \alpha T_c(r)}, \quad (1)$$

where $T_c(r)$ is the midplane temperature of the disk

at radius r and K is a constant with the value $K \equiv \sqrt{GM_*\mu m_p}/3\pi k$. Here μ is the mean molecular weight in units of the proton mass m_p , G is the gravitational constant, k is Boltzmann’s constant and M_* is the stellar mass. As we will show in Section 3, most of the disk is ‘irradiation-dominated’, and consequently has temperature given approximately by $T_c \sim r^{-1/2}$. This results in the surface density going as $\Sigma \sim r^{-1}$. This surface density distribution is less steep than the so-called ‘‘minimum mass solar nebula’’ (MMSN), given by $\Sigma \sim r^{-3/2}$ (Weidenschilling, 1977; Hayashi, 1981). Strictly, the MMSN does not necessarily represent the mass distribution at any instant, but the minimum mass that has passed through the disk during its lifetime (Lissauer, 1993, and references therein).

In reality protoplanetary disks are not quite steady. After the main infall phase is over, the disk is not supplied anymore with new matter, and the continuing accretion onto the star will drain matter from the disk (see Fig. 1). In addition the disk viscously expands and is subject to photoevaporation (see Section 5). The timescale for ‘‘viscous evolution’’ depends on radius and is given by $t_{\text{vis}} \simeq r^2/\nu$, which for typical CTTS parameters is 1 Myr at $r \simeq 100$ AU. Since for irradiated disks $t_{\text{vis}} \propto r$, the outer regions evolve the slowest, yet they contain most of the mass. These regions ($\gtrsim 50 - 100$ AU) therefore form a reservoir of mass constantly resupplying the inner regions. The latter can thus be approximately described by steady accretion disk models.

There might also be dramatic variability taking place on shorter timescales, as shown by FU Ori and EX Lupi type outbursts (Gammie and Johnson, 2005, and references therein). These outbursts can have various triggering mechanisms, such as thermal instability (Kawazoe and Mineshige, 1993; Bell and Lin, 1994); close passage of a companion star (Bonnell and Bastien 1992; Clarke and Syer, 1996); mass accumulation in the dead zone followed by gravitational instability (Gammie, 1996; Armitage et al., 2001). Disks are therefore quite time-varying, and constant α steady disk models should be taken as zeroth-order estimates of the disk structure.

Given the challenges of understanding the disk viscosity from first principles, attempts have been made to find observational constraints on disk evolution (Ruden and Pollock, 1991; Cassen, 1996; Hartmann et al., 1998; Stepinski, 1998). For example, Hartmann et al. (1998) study a large sample of CTTSs and find a decline in mass accretion rate with time, roughly described as $\dot{M} \sim t^{-1.5}$, which they compare to the analytic similarity solutions of Lynden-Bell and Pringle (1974) for the expanding disk. A similar type of observational constraint is the recently found rough correlation $\dot{M} \propto M_*^2$ (Muzerolle et al., 2003a, 2005; Natta et al., 2004). High angular resolution mm-wave continuum imaging can also help to constrain the mass surface density distribution. With this technique Wilner et al. (2000) concluded that $\Sigma \propto r^{-1}$ for TW Hydra. Kitamura et al. (2002) find $\Sigma \sim r^{-p}$, with $p = 0 - 1$ for a sample of T Tauri stars.

3. VERTICAL STRUCTURE OF DUSTY DISKS

With the radial structure following from accretion physics, as described above, the next issue is the vertical structure of these disks. Many authors have modeled this with full time-dependent 2D/3D (magneto/radiation-) hydrodynamics (e.g., Boss, 1996, 1997; Yorke and Bodenheimer, 1999; Fromang et al., 2004). While this approach is obviously very powerful, it suffers from large computational costs, and often requires strong simplifying assumptions in the radiative transfer to keep the problem tractable. For comparison to observed spectra and images these models are therefore less practical. Most observation-oriented disk structure models split the disk into a series of (nearly independent) annuli, each constituting a 1-D or a two-layer local vertical structure problem. In this section we review this kind of ‘1+1D’ models, and their 2-D/3-D generalizations.

3.1. Basic principles

The main objective of the models described in this section is the determination of the density and temperature structure of the disk. For a given surface density $\Sigma(r)$, and a given gas temperature structure $T_g(r, z)$ (where z is the vertical coordinate measured upward from the midplane) the vertical density distribution $\rho(r, z)$ can be readily obtained by integrating the vertical equation of hydrostatics:

$$\frac{dP}{dz} = -\rho\Omega_K^2 z \quad (2)$$

where $P = \rho c_s^2$ with $c_s^2 \equiv kT_g/\mu m_p$. The main complexity of a disk model lies in the computation of the temperature structure. Since the main source of opacity is the dust, most models so far make the assumption that the gas temperature is equal to the dust temperature, so that the gas temperature determination reduces to solving a dust continuum radiative transfer problem. In Section 4 we will relax this assumption, but until then we will keep it.

The temperature of the disk is set by a balance between heating and cooling. The disk cools by thermal emission from the dust grains at infrared wavelengths. This radiation is what is observed as infrared dust continuum radiation from such disks. Line cooling is only a minor coolant, and only plays a role for T_g when gas and dust are thermally decoupled. Dust grains can be heated in part by radiation from other grains in the disk. The iterative absorption and re-emission of infrared radiation by dust grains in the disk causes the radiation to propagate through the disk in a diffusive way. Net energy input comes from absorption of direct stellar light in the disk’s surface layers, and from viscous dissipation of gravitational energy in the disk due to accretion. For most disks around CTTSs and Herbig Ae/Be stars the heating by stellar radiation is dominant over the viscous heating (except in the very inner regions). Only for strongly accreting disks does the latter dominate.

Once the temperature structure is determined, the SED can be computed. The observable thermal emission of a dusty disk model consists of three wavelength regions (see

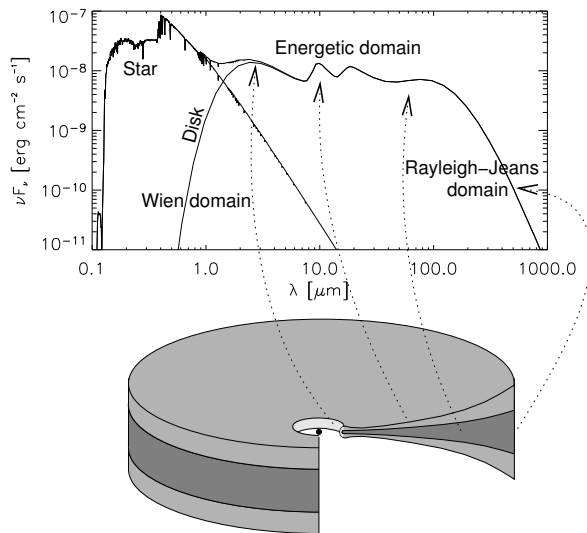


Fig. 2.— Build-up of the SED of a flaring protoplanetary disk and the origin of various components: the near-infrared bump comes from the inner rim, the infrared dust features from the warm surface layer, and the underlying continuum from the deeper (cooler) disk regions. Typically the near- and mid-infrared emission comes from small radii, while the far-infrared comes from the outer disk regions. The (sub-)millimeter emission mostly comes from the midplane of the outer disk. Scattering is not included here.

Fig. 2). The main portion of the energy is emitted in a wavelength range depending on the minimum and maximum temperature of the dust in the disk. We call this the “energetic domain” of the SED, which typically ranges from 1.5 μm to about 100 μm . At shorter wavelength the SED turns over into the “Wien domain”. At longer wavelengths the SED turns over into the “Rayleigh-Jeans domain”, a steep, nearly powerlaw profile with a slope depending on grain properties and disk optical depth (see chapter by Natta et al.). Differences in disk geometry are mainly reflected in the energetic domain of the SED, while the submm and mm fluxes probe the disk mass.

3.2. A first confrontation with observations

It is quite challenging to solve the entire disk structure according to the above principles. Early disk models were therefore often based on strong simplifications. An example of such a model is a perfectly flat disk being irradiated by the star due to the star’s non-negligible size (Adams and Shu, 1986; Friedjung, 1985). The stellar radiation impinges onto the flat disk under an irradiation angle $\varphi \simeq 0.4r_*/r$ (with r_* the stellar radius). Neglecting viscous dissipation, the effective temperature of the disk is set by a balance between the irradiated flux $(1/2)\varphi L_*/4\pi r^2$ (with L_* the stellar luminosity) and blackbody cooling σT_{eff}^4 , which yields $T_{\text{eff}} \propto r^{-3/4}$. The energetic domain of its SED therefore has a slope of $\nu F_\nu \propto \nu^s$ with $s = 4/3 = 1.33$, which

follows from the fact that any disk with $T_{\text{eff}} \propto r^{-q}$ has an SED slope of $s = (4q - 2)/q$. This steep slope arises because most of the stellar radiation is absorbed and re-emitted at small radii where the disk is hot. This produces strong emission at short wavelength. The long wavelength flux is weak because only little stellar radiation is absorbed at large radii. Observations of CTTs, however, show SED slopes typically in the range $s = 0.6$ to 1 (Kenyon and Hartmann, 1995), i.e. much less steep. The SEDs of Herbig Ae/Be stars show a similar picture, but with a somewhat larger spread in s , though it must be kept in mind that the determination of the slope of a bumpy SED like in Fig. 2 is somewhat subjective. Meeus et al. (2001, henceforth M01) divide the SEDs of Herbig Ae/Be stars into two groups: those with strong far-infrared flux (called ‘group I’, having slope $s \simeq -1 \dots 0.2$) and those with weak far-infrared flux (called ‘group II’, having slope $s \simeq 0.2 \dots 1$). All but the most extreme group II sources have a slope that is clearly inconsistent with that of a flat disk. Note, at this point, that the Meeus ‘group I’ and ‘group II’ are unrelated to the Lada ‘class I’ and ‘class II’ classification (both Meeus group I and II are members of Lada class II).

A number of authors have employed another model to interpret their observations of protoplanetary disks: that of a steady accretion disk heated by viscous dissipation (Rucinski et al., 1985; Bertout et al., 1988; Hillenbrand et al., 1992). These models are based on the model by Shakura and Sunyaev (1973). A detailed vertical structure model of such a disk was presented by Bell et al. (1997). The luminosity of such disks, including the magnetospheric accretion column, is $L_{\text{accr}} = GM_*\dot{M}/r_*$. For $r \gg r_{\text{in}}$ the effective temperature of such disks is given by $\sigma T_{\text{eff}}^4 = 3\dot{M}\Omega_K^2/8\pi$ (with σ the Stefan-Boltzmann constant), yielding an SED slope of $s = 4/3$, like for passive flat disks (Lynden-Bell, 1969; see solid lines of Fig. 6). Therefore these models are not very successful either, except for modeling very active disks like FU Orionis (FUor) outbursts (see Bell and Lin, 1994).

3.3. Flaring disk geometry

It was recognized by Kenyon and Hartmann (1987) that a natural explanation for the strong far-infrared flux (i.e. shallow SED slope) of most sources is a flaring (“bowl-shaped”) geometry of the disk’s surface, as depicted in Fig. 2. The flaring geometry allows the disk to capture a significant portion of the stellar radiation at large radii where the disk is cool, thereby boosting the mid- to far-infrared emission.

The flaring geometry adds an extra term to the irradiation angle: $\varphi \simeq 0.4r_*/r + rd(H_s/r)/dr$ (Chiang and Goldreich, 1997, henceforth CG97), where H_s is the height above the midplane where the disk becomes optically thick to the impinging stellar radiation. In the same way as for the flat disks the thermal balance determines the T_{eff} of the disk, but this now depends strongly on the shape of the disk: $H_s(r)$. The pressure scale height H_p , on the other hand, depends on the midplane temperature T_c by $H_p = \sqrt{kT_cr^3/\mu m_p GM_*}$

(with M_* the stellar mass). If we set $T_c = T_{\text{eff}}$ and if the ratio $\chi \equiv H_s/H_p$ is known, then the system of equations is closed and can be solved (see appendix *Chiang et al.*, 2001). For the special case that χ is constant we obtain $H_s \propto r^{9/7}$, a-posteriori confirming that the disk indeed has a “bowl” shape. In general, though, χ must be computed numerically, and depends on the dust opacity of the disk upper layers. The resulting temperature profile is typically about $T_c \propto r^{-0.5}$.

The total luminosity of such a non-accreting flaring disk is $L_{\text{disk}} = C L_*$, where C is the *covering fraction* of the disk. The covering fraction is the fraction of the starlight that is captured by the material in the disk. With a large enough disk inner radius ($r_{\text{in}} \gg r_*$) one can write $C \simeq \max(H_s(r)/r)$. For an infinitely thin disk extending from r_* to $r \rightarrow \infty$ one has $C = 0.25$. The *observed* flux ratio F_{disk}/F_* may deviate from C by about a factor of 2 due to the anisotropy of disk emission.

In addition to irradiation by the star, the outer regions of a strongly accreting flaring disk (like an FUor object) can also be irradiated by the accretion luminosity from the inner disk (*Kenyon and Hartmann*, 1991; *Bell*, 1999; *Lachaume*, 2004) and by the emission from the magnetospheric accretion column or boundary layer (*Muzerolle et al.*, 2003b).

3.4. Warm dust surface layer

A closer look at the physics of an irradiation-dominated disk (be it flat or flared) reveals that its surface temperature is generally higher than its interior temperature (*Calvet et al.*, 1991; *Malbet and Bertout*, 1991; CG97). Dust grains in the surface layers are directly exposed to the stellar radiation, and are therefore hotter than dust grains residing deep in the disk which only ‘see’ the infrared emission by other dust grains. The temperature difference is typically a factor of 2 – 4 for non/weakly-accreting disks (see curve labeled “-9” in Fig. 4). For non-negligible accretion, on the other hand, the disk is heated from inside as well, producing a temperature minimum somewhere between the equatorial plane and the surface layer (see other curves in Fig. 4). Because of the shallow incidence angle of the stellar radiation $\varphi \ll 1$, the *vertical* optical depth of this warm surface layer is very low. The layer produces optically thin emission at a temperature higher than the effective temperature of the disk. The frequency-integrated flux of this emission is the same as that from the disk interior. As a consequence, the thermal radiation from these surface layers produces dust features in *emission*. This is exactly what is seen in nearly all non-edge-on T Tauri and Herbig Ae/Be star spectra (e.g. M01; *Kessler-Silacci et al.*, 2006), indicating that these disks are nearly always dominated by irradiation.

3.5. Detailed models for flaring disks

3.5.1. Disk structure. Armed with the concepts of disk flaring and hot surface layers, a number of authors published detailed 1+1D disk models and two-layer (surface+interior) models with direct applicability to observa-

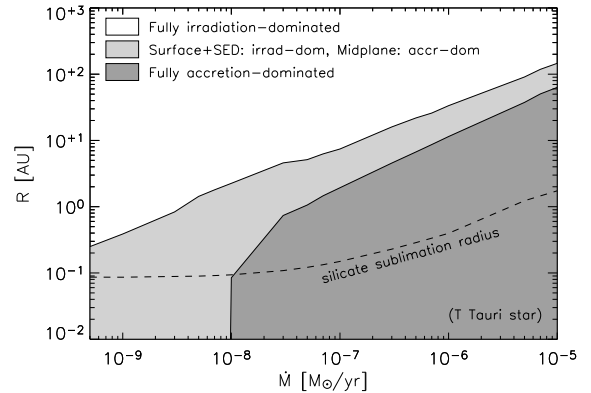


Fig. 3.— Characteristic radii of a disk around a $0.9 M_{\odot}$ star with $T_* = 4000$ K and $R_* = 1.9 R_{\odot}$ at different accretion rates. The silicate sublimation radius is the dust ‘inner rim’. Figure based on models by *D’Alessio et al.* (1998).

tions. The aforementioned CG97 model (with refinements described in *Chiang et al.*, 2001) is a handy two-layer model for the interpretation of SEDs and dust emission features from *non-accreting* (‘passive’) disks. *Lachaume et al.* (2003) extended it to include viscous dissipation.

The models by *D’Alessio et al.* (1998) solve the complete 1+1D disk structure problem with diffusive radiative transfer, including stellar irradiation and viscous dissipation (using the α prescription). The main input parameters are a global (constant) mass accretion rate \dot{M} and α . The surface density profile $\Sigma(r)$ is calculated self-consistently. This model shows that the disk can be divided into three zones: an outer zone in which the disk is dominated by irradiation, an inner zone where viscous dissipation dominates the energy balance, and an intermediate zone where the midplane temperature is dominated by the viscous dissipation but the surface temperature by irradiation (See Fig. 3). In the intermediate zone the vertical disk thickness is set by \dot{M} and α but the infrared spectrum is still powered by irradiation. In Fig. 4 the vertical structure of the disk is shown, for fixed Σ but varying \dot{M} for $r = 1$ AU.

The models described by *Dullemond, et al.* (2002) apply exact 1-D wavelength-dependent radiative transfer for the vertical structure, but these models do not include viscous dissipation.

3.5.2. Dust growth and sedimentation. Models of the kind discussed above describe the SEDs of CTTSs reasonably well. However, *D’Alessio et al.* (1999) argue that they tend to slightly overproduce far-infrared flux and have too thick dark lanes in images of edge-on disks. They also show that the percentage of expected edge-on disks appears to be overpredicted. They suggest that dust sedimentation could help to solve this problem. *Chiang et al.* (2001) find similar results for a subset of their Herbig Ae/Be star sample: the Meeus group II sources (see also CG97). They fit these sources by mimicking dust settling through a reduction of

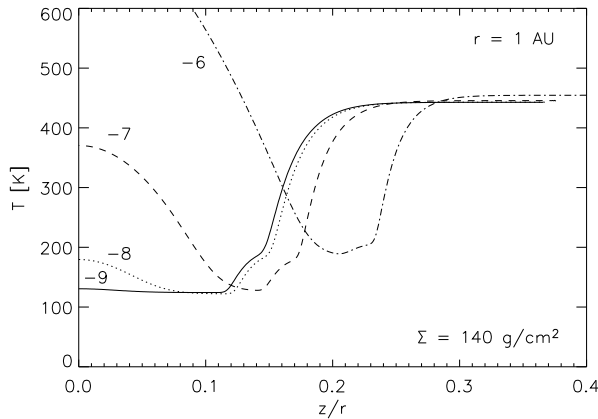


Fig. 4.— Vertical temperature distribution of an irradiated α -disk at 1 AU, for a fixed Σ (chosen to be that of a disk model with $\dot{M} = 10^{-8} M_{\odot}/\text{yr}$ for $\alpha = 0.01$), but varying \dot{M} , computed using the models of *D’Alessio et al.* (1998). The labels of the curves denote the 10-log of the accretion rate in M_{\odot}/yr .

the disk surface height. Self-consistent computations of dust sedimentation produce similar SEDs and confirm the dust settling idea (*Miyake and Nakagawa, 1995; Dullemond and Dominik, 2004b*, henceforth DD04b; *D’Alessio et al., 2006*). The disk thickness and far-infrared flux can also be reduced by grain growth (*D’Alessio et al., 2001; Dullemond and Dominik, 2004a*). The chapter by *Dominik et al.* discusses such models of grain growth and sedimentation in detail.

From comparing infrared and (sub-)millimeter spectra of the same sources (*Acke et al., 2004*), it is clear that small and big grains co-exist in these disks. The (sub-)millimeter spectral slopes usually require mm-sized grains near the midplane in the outer regions of the disk, while infrared dust emission features clearly prove that the disk surface layers are dominated by grains no larger than a few microns (see chapter by *Natta et al.*). It appears that a bimodal grain size distribution can fit the observed spectra: a portion of sub-micron grains in the surface layers responsible for the infrared dust emission features and a portion of mm-sized grains in the disk interior accounting for the (sub-)millimeter emission (*Natta et al., 2001*).

3.6. The dust ‘inner rim’

The very inner part of the disk is dust-free due to dust sublimation (see chapter by *Najita et al.* for a discussion of this region). The dusty part of the disk can therefore be expected to have a relatively abrupt inner edge at about 0.5 AU for a $50 L_{\odot}$ star (scaling roughly with $\sqrt{L_{*}}$). If the gas inward of this dust inner rim is optically thin, which appears to be mostly the case (*Muzerolle et al., 2004*), then this dust inner rim is illuminated by the star at a ~ 90 degree angle, and is hence expected to be much hotter than the rest of the disk behind it which is irradiated under a shallow angle

$\varphi \ll 1$. (*Natta et al., 2001*). Consequently it must be hydrostatically ‘puffed-up’, although this is still under debate. *Natta et al. (2001)* showed that the emission from such a hot inner rim can explain the near-infrared bump seen in almost all Herbig Ae/Be star SEDs (see e.g., M01). This is a natural explanation, since dust sublimation occurs typically around 1500 K, and a 1500 K blackbody bump fits reasonably well to the near-infrared bumps in those sources. *Tuthill et al. (2001)* independently discovered a bright half-moon ring around the Herbig Be star LkHa-101, which they attribute to a bright inner disk rim due to dust sublimation. *Dullemond et al. (2001; henceforth DDN01)* extended the CG97 model to include such a puffed-up rim, and *Dominik et al. (2003)* showed that the Meeus sample of Herbig Ae/Be stars can be reasonably well fitted by this model. However, for Meeus group II sources these fits required relatively small disks (see, however, Section 3.7).

The initial rim models were rather simplified, treating it as a vertical blackbody ‘wall’ (DDN01). *Isella and Natta (2005)* improved this by noting that the weak dependence of the sublimation temperature on gas density is enough to strongly round off the rim. Rounded-off rims appear to be more consistent with observations than the vertical ones: their flux is less inclination dependent, and their images on the sky are not so much one-sided. There is still a worry, though, whether the rims can be high enough to fit sources with a strong near-infrared bump.

With near-infrared interferometry the rim can be spatially resolved, and thus the models can be tested. The measurements so far do not yet give images, but the measured ‘visibilities’ can be compared to models. In this way one can measure the radius of the rim (e.g., *Monnier et al., 2005; Akeson et al., 2005*) and its inclination (e.g., *Eisner et al., 2003*). Moreover it can test whether indeed the near-infrared emission comes from the inner rim of the dust disk in the first place (some doubts have been voiced by *Vinkovic et al., 2003*). We refer to the chapter by *Millan-Gabet et al.* for a more in-depth discussion of interferometric measurements of disks.

The inner rim model has so far been mainly applied to Herbig Ae/Be stars because the rim appears so apparent in the near-infrared (NIR). But *Muzerolle et al. (2003b)* showed that it also applies to T Tauri stars. In that case, however, the luminosity from the magnetospheric accretion shock is required in addition to the stellar luminosity to power the inner rim emission.

In addition to being a strong source of NIR flux, the ‘puffed-up’ inner dust rim might also be responsible for the irregular few-day-long extinction events observed toward UX Orionis stars (*Natta et al. 2001; Dullemond et al. 2003*). The latter authors argued that this only works for self-shadowed (or only weakly flaring) disks (see Section 3.7).

In Fig. 5 we summarize in a qualitative way how the disk geometry (inner rim, flaring) affects the SED shape of an irradiated passive disk. In Fig. 6 the SEDs of actively accreting disks are shown, in which the irradiation by the central

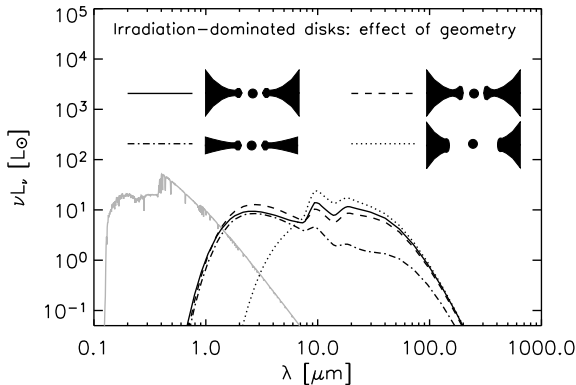


Fig. 5.— Overall SED shape for *non-accreting* disks with stellar irradiation, computed using the 2-D radiative transfer tools from *Dullemond & Dominik (2004a)*. The stellar spectrum is added in grey-scale. Scattered light is not included in these SEDs. Solid line is normal flaring disk with inner dust rim; dashed line is when the rim is made higher; dot-dashed line is when the flaring is reduced (or when the disk becomes ‘self-shadowed’); dotted line is when the inner rim is at $10\times$ larger radius.

star is ignored. In reality, both the accretional heating and the irradiation by the central star must be included in the models simultaneously.

3.7. 2-D radiative transfer in disk models

The models described so far are all based on an approximate 1+1D (or two-layer) irradiation-angle description. In reality the structure of these disks is 2-D, if axisymmetry can be assumed, and 3-D if it cannot. Over the last 10 years many multi-dimensional dust continuum radiative transfer programs and algorithms were developed for this purpose (e.g., *Whitney et al., 1992; Lucy et al., 1999; Wolf et al., 1999; Bjorkman and Wood, 2001; Nicolini et al., 2003; Steinacker et al., 2003*). Most applications of these codes assume a given density distribution and compute spectra and images. There is a vast literature on such applications which we will not review here (see chapter by *Watson et al.*). But there is a trend to include the self-consistent vertical density structure into the models by iterating between radiative transfer and the vertical pressure balance equation (*Nomura, 2002; Dullemond, 2002*, henceforth D02; *Dullemond and Dominik, 2004a*, henceforth DD04a; *Walker et al., 2004*). The main improvements of 2-D/3-D models over 1+1D models is their ability to account for radial radiative energy diffusion in the disk, for cooling of the outer disk in radial direction, for the complex 3-D structure of the dust inner rim, and in general for more realistic model images.

In addition to this, 2-D/3-D models allow for a ‘new’ class of disk geometries to be investigated. The 1+1D models can, because of their reliance on an irradiation angle φ , only model disk geometries that are either flat or flared.

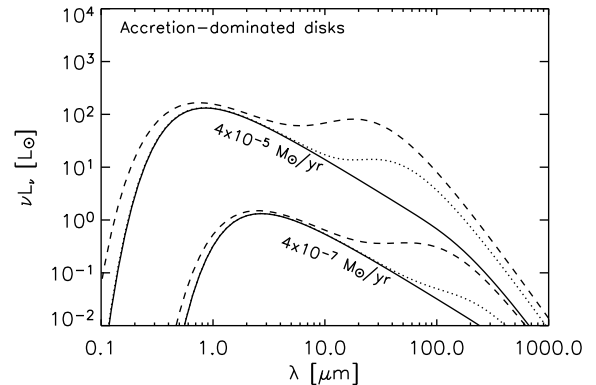


Fig. 6.— Overall SED shape for accreting disks *without* stellar irradiation for two accretion rates. A simple Shakura-Sunyaev model is used here with grey opacities. Solid line: pure Shakura-Sunyaev model (star not included); dotted line: model with disk-self-irradiation included; dashed line: model with disk-self-irradiation *and* irradiation by the magnetospheric accretion column on the star included.

In principle, however, there might be circumstances under which, roughly speaking, the surface of the outer disk regions lies within the shadow of the inner disk regions (although the concept of ‘shadow’ must be used with care here). These shadowed regions are cooler than they would be if the disk was flaring, but the 2-D/3-D nature of radiative transfer prevents them from becoming entirely cold and flat. For Herbig Ae/Be stars the origin of the shadow might be the puffed-up inner rim (D02, DD04a), while for T Tauri stars it might be the entire inner flaring disk region out to some radius (DD04b).

Although the concept of ‘self-shadowing’ is still under debate, it might be linked to various observable features of protoplanetary disks. For instance, DD04a showed that self-shadowed disks produce SEDs consistent with Meeus group II sources, while flaring disks generally produce group I type SEDs, unless the disk outer radius is very small. It might also underly the observed correlation between SED shape and sub-millimeter slope (*Acke et al. 2004*). Moreover, self-shadowed disks, when spatially resolved in scattered light, would be much dimmer than flaring disks.

4. GAS TEMPERATURE AND LINE SPECTRA

Although the dust in disks is generally more easily observed, there is an obvious interest in direct observations of the gas. It dominates the mass, sets the structure and impacts dust dynamics and settling in these disks. Moreover, it is important to estimate how long disks remain gas-rich, and whether this is consistent with the formation time scale of gas giant planets (*Hubickyj et al., 2004*). Unfortunately, gas lines such as CO rotational, H₂ rotational and atomic fine

structure lines often probe those surface regions of disks in which the gas temperature is difficult to compute. The disk models we described above assume that the gas temperature in the disk is always equal to the local dust temperature. While this is presumably true for most of the matter deep within optically thick disks, in the tenuous surface layers of these disks (or throughout optically thin disks) the densities become so low that the gas will thermally decouple from the dust. The gas will acquire its own temperature, which is set by a balance between various heating- and cooling processes. These processes depend strongly on the abundance of various atomic and molecular species, which, for their part, depend strongly on the temperature. The gas temperature, density, chemistry, radiative transfer and radiation environment are therefore intimately intertwined and have to be studied as a single entity. This greatly complicates the modeling effort, and the first models which study this in detail have only recently been published.

This chapter focuses on stationary models, i.e. models that are in chemical, thermal and hydrostatic equilibrium. For the tenuous regions of disks the chemical time scales are short enough that this is valid, in contrast to the longer chemical time scales deeper in the disk (e.g., *Aikawa and Herbst*, 1999; *Willacy et al.*, 2000). The models constructed so far either solve the gas temperature/chemistry for a fixed gas density structure (*Jonkheid et al.*, 2004; *Kamp and Dullemond*, 2004), or include the gas density in the computation to obtain a self-consistent thermo-chemical-hydrostatic structure (*Gorti and Hollenbach*, 2004; *Nomura and Millar*, 2005).

4.1. Basic gas physics

The physics and chemistry of the surface layers of protoplanetary disks strongly resembles that of photon dominated regions (PDRs, *Tielens and Hollenbach*, 1985; *Yamashita et al.* 1993). In those surface layers the gas temperature generally greatly exceeds the dust temperature. But the dust-gas coupling gradually takes over the gas temperature balance as one gets deeper into the disk, typically beyond a vertical column depth of $A_V \simeq 1$, and forces the gas temperature to the dust temperature.

The uppermost surface layer contains mostly atomic and ionized species, since the high UV irradiation effectively dissociates all molecules (*Aikawa et al.*, 2002). The photochemistry is driven by the stellar UV irradiation and/or in case of nearby O/B stars, by external illumination. In flaring disk models, the stellar UV radiation penetrates the disk under an irradiation angle φ like the one described in the previous section. This radiation gets diluted with increasing distance from the central star and attenuated by dust and gas along an *inclined* path into the disk. The stellar UV radiation therefore penetrates less deep into the disk than external UV radiation. As one goes deeper into the surface layer, the gas becomes molecular (see chapter by *Bergin et al.*).

The thermal balance of the gas in disks is solved by

equating all relevant heating and cooling processes. For this gas thermal balance equation, a limited set of key atomic and molecular species is sufficient: e.g., H_2 , CO, OH, H_2O , C^+ , O, Si^+ and various other heavy elements. For most atoms and molecules, the statistical equilibrium equation has to include the pumping of the fine structure and rotational levels by the cosmic background radiation, which become important deep in the disk, where stellar radiation cannot penetrate. The full radiative transfer in chemical models is very challenging, and therefore generally approximated by a simple escape probability approach, where the pumping and escape probability are derived from the optical depth of the line (similar to the approach of *Tielens and Hollenbach*, 1985 for PDRs). Even though the emitted photons travel in all directions, the optical depth used for this escape probability is the line optical depth in the *vertical* direction where the photons most readily escape.

One of the most critical ingredients of these models is the UV and X-ray radiation field (stellar and external), which can be split into the far-ultraviolet (FUV, 6-13.6 eV), the extreme-ultraviolet (EUV, 13.6-100 eV) and X-ray ($\gtrsim 100$ eV) regime. In the literature the far ultraviolet radiation field (FUV) is often represented by a single parameter G_0 describing the integrated intensity between 912 and 2000 Å normalized to that of the typical interstellar radiation field (*Habing*, 1968). However, several papers have shown the importance of a more detailed description of the radiation field for calculations of the chemistry and the gas heating/cooling balance (*Spaans et al.*, 1994; *Kamp & Bertoldi*, 2000; *Bergin et al.*, 2003; *Kamp et al.*, 2006; *Nomura and Millar*, 2005). For instance, in T Tauri stars the radiation field is dominated by strong Ly α emission, which has consequences for the photodissociation rate of molecules that can be dissociated by Ly α photons. The photoelectric heating process, on the other hand, depends strongly on the overall shape of the radiation field, which is much steeper in the case of cool stars. A similar problem appears in the X-ray spectra of cool M stars, which are dominated by line emission.

FUV induced grain photoelectric heating is often a dominant heating process for the gas in the irradiated surface layers. The FUV photon is absorbed by a dust grain or a polycyclic aromatic hydrocarbon (PAH) molecule, which ejects an energetic electron to the gas, and heats the gas via the thermalization of the energetic electron. Its efficiency and thus the final gas temperature depends strongly on the grain charge, dust grain size and composition (PAHs, silicates, graphites, ices, etc.). X-rays from the central star also heat only the uppermost surface layers, as their heating drops off monotonically with column, and gets quite small by columns of order 10^{21} cm^{-2} .

4.2. Surfaces of optically thick disks

This subsection focuses on the warm surface layers of the optically thick disk at $A_V < 1$, measured vertically downwards, where gas and dust temperatures decouple.

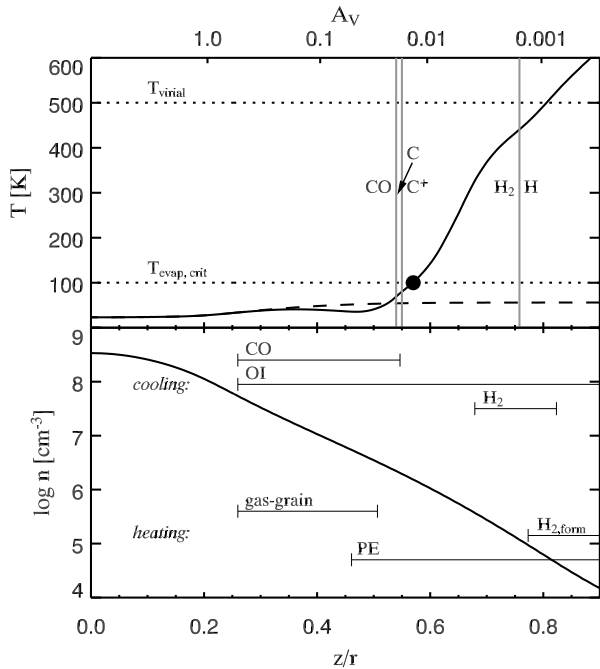


Fig. 7.— Upper panel: gas (solid line) and dust (dashed line) temperatures in a vertical cut through the T Tauri star model at 100 AU. Overplotted are the most important chemical transitions from atomic to molecular species. The black filled circle shows the point where a photoevaporative flow can be initiated (see Section 5). Lower panel: same vertical cut for the hydrogen number density (fixed input density distribution). Overplotted are the ranges over which the respective heating/cooling processes contribute more than 10% to the total heating/cooling rate at that depth (‘PE’ means photoelectric heating; ‘H_{2,form}’ means heating through molecular hydrogen formation; see Section 5 for the definition of $T_{\text{evap,crit}}$ and T_{virial}).

Modeling of these surface layers is not affected by the optically thick disk interior and depends mainly on the local UV/X-ray flux and the gas density. The typical hydrogen gas number density in these layers is roughly $n_H(A_V = 1) \simeq 10^7 (100 \text{ AU}/r) \delta^{-1} \text{ cm}^{-3}$. The location of the $A_V = 1$ surface depends on the ratio δ of the dust surface area per hydrogen nucleus to the interstellar value, which is roughly $10^{-21} \text{ cm}^2/\text{H}$. Assuming a surface density that drops linearly with radius and $\Sigma(1 \text{ AU}) = 1000 \text{ g cm}^{-2}$, the fractional column density $\Sigma_{\text{surf}}/\Sigma$ contained in the surface layer ($T_{\text{gas}} \neq T_{\text{dust}}$) is usually small, $\Sigma_{\text{surf}}/\Sigma \simeq 1.5 \times 10^{-6} \delta^{-1} (r/\text{AU})$, but increases linearly with radius.

4.2.1. Gas temperatures. The detailed temperature structure of the surface layers of optically thick young disks was studied for the first time by *Jonkheid et al.* (2004), *Kamp and Dullemond* (2004), and *Nomura and Millar* (2005). These models neglect EUV irradiation and start with neutral hydrogen in the top layers. Fig. 7 shows the vertical

structure in a disk model with $0.01 M_{\odot}$ at 100 AU around a $0.5 M_{\odot}$ T Tauri star (from models of *Kamp and Dullemond*, 2004; note that the density structure in these models is not iterated with the gas temperature). Very high in the atmosphere at particle densities as low as $n < 10^5 \text{ cm}^{-3}$ ($A_V \lesssim 10^{-3}$), the gas temperature is set by a balance between photoelectric heating and fine structure line cooling of neutral oxygen (*Kamp and Dullemond*, 2004; *Jonkheid et al.*, 2004). This leads to gas temperatures of several hundred K. Deeper in the disk, for $A_V > 0.01$, molecules can shield themselves from the dissociating FUV radiation. As soon as the fraction of molecular hydrogen becomes larger than 1%, H₂ line cooling becomes important. Molecular line emission – mainly CO and H₂ – cools the gas down to below hundred K before the densities are high enough for gas and dust to thermally couple. As gas temperatures drop below ~ 100 K, H₂ no longer contributes to the cooling. Instead CO, which has a rich rotational spectrum at low temperatures, becomes an important coolant. At larger radii the FUV flux from the central star drops as well as the density of the surface layer, leading to lower gas temperatures. At distances $r \gtrsim 100$ AU the gas temperature is too low for the endothermic destruction of H₂ by O atoms and hence the surface layer at those distances contains substantial fractions of molecular hydrogen.

4.2.2. Implications for the disk structure. Detailed models of the gas temperature have shown that gas and dust are collisionally coupled at optical depth $A_V > 1$. Thus the basic assumption $T_{\text{gas}} = T_{\text{dust}}$ of the disk structure models presented in the previous section is justified for the disk interior. The main effect of the higher gas temperatures in the warm surface layer is an enhanced flaring of the disk (*Nomura and Millar*, 2005).

4.2.3. Observations and comparison with models. The pure rotational lines of H₂ such as $J = 2 - 0 \text{ S}(0)$ [$28 \mu\text{m}$], $J = 3 - 1 \text{ S}(1)$ [$17 \mu\text{m}$], $J = 4 - 2 \text{ S}(2)$ [$12 \mu\text{m}$] and $J = 6 - 4 \text{ S}(4)$ [$8 \mu\text{m}$] trace the warm gas (100-200 K) in the disks. Even though there is some controversy about detection of those lines with different instruments (*Thi et al.*, 2001; *Richter et al.*, 2002), there is a tentative detection of H₂ in AB Aurigae using the Texas Echelon Cross Echelle Spectrograph (TEXES) at the Infrared Telescope Facility (*Richter et al.*, 2002). *Bary et al.* (2003) report $v = 1 - 0 \text{ S}(1)$ [$2.12 \mu\text{m}$] emission in high resolution spectra ($R \sim 60\,000$) of the T Tauri stars GG Tau A, LkCa 15, TW Hya and DoAr21. This emission most likely arises in the low density, high temperature upper surfaces beyond 10 AU. According to the disk models, warm H₂ exists indeed in the optically thin surface layers, where $T_{\text{gas}} \gg T_{\text{dust}}$ and the observed fluxes can be reproduced (*Nomura and Millar*, 2005). Fig. 8 reveals the effect of UV fluorescence on the line strength. The UV fluorescent lines, which are an excellent probe of the inner disk ($r < \text{few AU}$), are discussed in detail in the chapter by Najita et al.. The detection of the mid-IR H₂ lines at low spectral resolution (e.g., with Spitzer) is hindered by

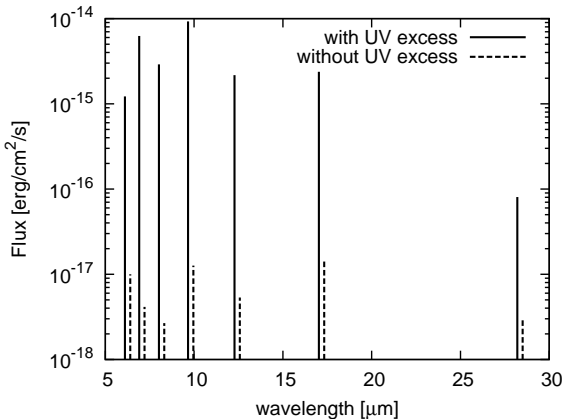


Fig. 8.— The mid-infrared line spectra of molecular hydrogen from a T Tauri disk model ($M_* = 0.5 M_\odot$, $R_* = 2 R_\odot$, $T_{\text{eff}} = 4000$ K, $\dot{M} = 10^{-8} M_\odot/\text{yr}$) with (solid line) and without (dotted line) UV excess (Nomura and Millar, 2005).

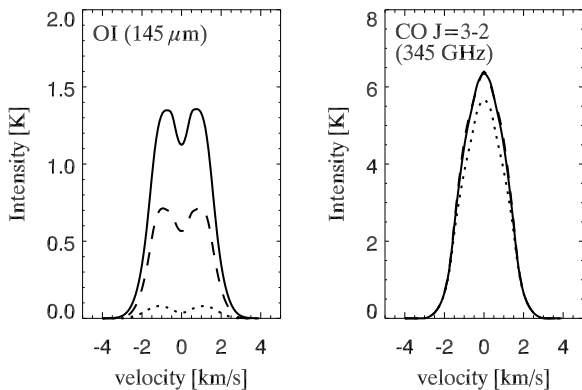


Fig. 9.— Impact of detailed gas temperature modeling and dust settling on the emission lines of oxygen and CO (Jonkheid et al. 2004): $T_{\text{gas}} = T_{\text{dust}}$ (dotted line), detailed gas energy balance (solid line), dust settling (dashed line).

the low line-to-continuum ratio.

The impact of detailed gas modeling differs for the various emission lines. CO, which forms deeper in the disk is generally less affected than fine structure lines such as [O I] and [C II] that form in the uppermost surface layers, where $T_{\text{gas}} \gg T_{\text{dust}}$ (Fig. 9). Since the gas temperature in those layers is set by photoelectric heating, dust settling leads to lower temperatures and thus to weaker line emission.

The [O I] 6300 Å line is another tracer of the physics in the tenuous surface layers (see also the chapter by Bergin et al.). It has been detected in a number of externally illuminated proplyds in the Orion nebula (Johnstone et al., 1998) as well as in T Tauri and Herbig Ae/Be stars (Acke et al., 2005; Acke and van den Ancker, 2006). Störzer and Hollenbach (1999) explain the emission in the Orion proplyds by the photodissociation of the OH molecule, which leaves about 50% of the atomic oxygen formed in the up-

per $^1\text{D}_2$ level of the 6300 Å line. Acke et al. (2005) find indication of Keplerian rotation from the [O I] line profiles. However, they need OH abundances higher than those predicted from disk models to fit the emission from the disks around Herbig Ae/Be stars. Gas models of those disks reveal the presence of a high temperature reservoir (few 1000 K); hence the [O I] line might arise partly from thermal excitation at radii smaller than 100 AU (Kamp et al., 2006). Resolved [O I] 6300 Å line emission from the disk around the Herbig Ae star HD 100546 (Acke and van den Ancker, 2006) shows that the emission is spread between ~ 1 and 100 AU and supports the presence of a gap at ~ 10 AU as reported initially by Bouwman et al. (2003).

4.3. Optically thin disks

As protoplanetary disks evolve, the dust grains grow to at least centimeter sizes and the disks become optically thin. In addition, as we shall discuss Section 5, the gas in the disk ultimately disappears, turning the disk into a debris disk. It is therefore theoretically conceivable that there exists a transition period in which the disk has become optically thin in dust continuum, but still contains a detectable amount of gas. The source HD141569 (5 Myr) might be an example of this, as Brittain et al. (2003) observed UV excited warm CO gas from the inner rim at ~ 17 AU, and Dent et al. (2005) cold gas further out ($J = 3 - 2$). Measuring the gas mass in such transition disks sets a timescale for the planet formation process. The Spitzer Legacy Science Program ‘Formation and Evolution of Planetary Systems’ (FEPS) has set upper limits on gas masses of $\sim 0.1 M_J$ around solar-type stars with ages greater than 10 Myr (Meyer et al., 2004; Hollenbach et al., 2005; Pascucci et al., 2005).

4.3.1. Disk models. Several groups have so far studied these transition phases of protoplanetary disks: Gorti and Hollenbach (2004) modeled the disk structure and gas/dust emission from intermediate aged disks around low-mass stars, Kamp and Bertoldi (2000), Kamp and van Zadelhoff (2001), and Kamp et al. (2003) modeled the gas chemistry and line emission from A-type stars such as β Pictoris and Vega. Jonkheid et al. (2006) studied the gas chemical structure and molecular emission in the transition phase disk around HD 141569 A. These models are all based on the same physics as outlined above for the optically thick protoplanetary disks. The disks are still in hydrostatic equilibrium, so that the disk structure in these low mass disks is similar to that in the more massive disks with the midplane simply removed. However, some fundamental differences remain: the minimum grain size in these disks is typically a few microns, much larger than in the young protoplanetary disks; in addition, the dust may have settled towards the midplane, and much of the solid mass may reside in larger particles ($a > 1$ cm) than can be currently observed. This reduces the grain opacity and the dust-to-gas mass ratio compared to the younger optically thick disks. At radial midplane gas column densities smaller than 10^{23} cm^{-2} , these disks are optically thin to stellar UV and ~ 1 keV X-

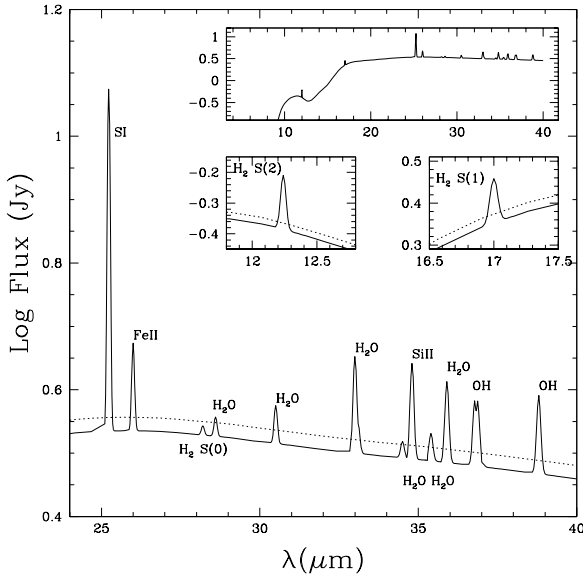


Fig. 10.— Mid-infrared spectrum in the 24 – 40 μm wavelength region showing the dust continuum and dominant gas emission lines for a disk model with $M_{\text{gas}} = 10^{-2} M_{\text{J}}$ and $M_{\text{dust}} = 10^{-5} M_{\text{J}}$ (with dust defined as particles smaller than 1 mm). A distance to the disk of 30 pc and a spectral resolving power $R = 600$ is assumed (Gorti and Hollenbach, 2004)

ray photons and the gas is mostly atomic. At radial columns greater than that, the gas opacity becomes large enough to shield H_2 and CO, allowing significant molecular abundances. For disks extended to 100 AU, very little mass (very roughly $\gtrsim 10^{-3} M_{\text{J}}$) is needed to provide this shielding.

4.3.2. Comparison with observations. Since the continuum remains optically thin, the mid-IR spectrum is dominated by fine-structure emission lines from ions such as [Fe II] and [Si II]; large columns of neutral sulphur are common, leading to strong [S I] emission (Fig. 10). However, the strength and thus detectability of these lines depends on the abundances of heavy metals in late phases of disk evolution, which is uncertain, especially the more refractory Fe. In the opaque molecular regions somewhat closer to the star, the gas temperature exceeds 100 K and molecular hydrogen emission is produced. The S(0) and S(1) H_2 lines stay optically thin over a large range of disk masses and *if detected* are more diagnostic of disk mass than other fine structure lines (Gorti and Hollenbach (2004)). While the strongest molecular bands of H_2O (important coolant in disk mid-plane) and OH are similar in strength to the fine structure lines, the H_2 lines are weak and detection can be significantly hampered by the low line-to-continuum ratio (weak narrow line against the bright dust thermal background). These mid-IR lines generally originate from 1–10 AU.

Kamp *et al.* (2003) have shown that beyond 40 AU the dominant coolant for the latest tenuous stages of disk evo-

lution is the [C II] 158 μm line. The fine structure lines of C, O and C^+ trace only the surface of these tenuous disks: [O I] becomes rapidly optically thick and C^+ and C turn into CO as soon as UV CO and H_2 bands become optically thick, and stellar UV cannot penetrate any further. Since typical gas temperatures are higher than in molecular clouds, CO lines from the upper rotational levels ($J = 4 - 3$) are predicted to be stronger than the lower J lines. Dent *et al.* (2005) have recently detected the CO $J = 3 - 2$ line in HD141569 and disk modeling by Jonkheid *et al.* (2006) shows that the profile excludes a significant contribution from gas inwards of ~ 80 AU and estimate the total gas mass to be $80 M_{\text{E}}$.

5. PHOTOEVAPORATION OF A DISK BY ITS CENTRAL STAR

5.1. Introduction

The above section has shown that in the surface layers of the disk the gas temperature can become very high, greatly exceeding the dust temperature. The warm surface gas can flow off the disk and escape the gravity of the star. Since the heating process responsible for these high temperatures is the *radiation* from the central star or a nearby O-star, this process is called “photoevaporation”. The viscous evolution (i.e. accretion and spreading) of the disk, discussed in Section 2, can be strongly affected by this photoevaporation process. Typically, it significantly shortens the ‘lifetime’ of a disk compared to pure viscous evolution. Photoevaporation can also create inner holes or truncate the outer disk. This has relevance to observations of such disks, such as the percentage of young stars with infrared excess versus their age (Haisch *et al.*, 2001; Carpenter *et al.*, 2005), or the inferred ‘large inner holes’ of some disks (e.g., Calvet *et al.*, 2002; Bouwman *et al.*, 2003; Forrest *et al.*, 2004; D’Alessio *et al.*, 2005). It has also far-reaching consequences for the formation of planets, as we will discuss below.

Photoevaporation has already been discussed in earlier reviews (Hollenbach *et al.*, 2000; Hollenbach and Adams, 2004; Richling *et al.*, 2006). However, these reviews mainly focused on the heating by a nearby massive star (such as the famous case of the proplyds in Orion). In contrast, in this section we will exclusively review recent results on photoevaporation by the central star, consistent with the previous sections which focus on heating and photodissociation by the central star. Progress in this field since PPIV has been mostly theoretical, since observations of diagnostic gas spectral lines for the case of photoevaporation by the central, low mass star requires greater sensitivity, spectral resolution, and spatial resolution than currently available. We will, however, discuss the implications for the observed ‘inner holes’ and disk lifetimes.

5.2. The Physics of Photoevaporation

5.2.1. Basic Concepts. Photoevaporation results when stellar radiation heats the disk surface and resulting thermal pressure gradients drive an expanding hydrodynamical flow

to space. As shown in Section 4 the main heating photons lie in the FUV, EUV and X-ray energy regimes. X-rays, however, were shown to be of lesser importance for photoevaporation (Alexander *et al.*, 2004b), and we will not consider them further.

There are two main sources of the strong EUV and FUV excesses observed in young low mass stars: accretion luminosity and prolonged excess chromospheric activity. Recent work (Alexander *et al.*, 2004a) has shown that EUV photons do not penetrate accretion columns, so that accretion cannot provide escaping EUV photons to power photoevaporation. Alexander *et al.* (2005) present indirect observational evidence that an active chromosphere may persist in T Tauri stars even without strong accretion, and that EUV luminosities of $\Phi_{\text{EUV}} > 10^{41}$ photons/s may persist in low mass stars for extended ($\gtrsim 10^{6.5} - 10^7$ yrs) periods to illuminate their outer disks. FUV photons may penetrate accretion columns and also are produced in active chromospheres. They are measured in nearby, young, solar mass stars with little accretion and typically (with great scatter) have luminosity ratios $L_{\text{FUV}}/L_{\text{bol}} \sim 10^{-3}$ or $\Phi_{\text{FUV}} \sim 10^{42}$ photons/s.

EUV photons ionize the hydrogen in the very upper layers of the disk and heat it to a temperature of $\sim 10^4$ K, independent of radius. FUV photons penetrate deeper into the disk and heat the gas to $T \sim 100 - 5000$ K, depending on the intensity of the FUV flux, the gas density and the chemistry (as was discussed in Section 4). Whether the EUV or FUV heating is enough to drive an evaporative flow depends on how the resulting thermal speed (or sound speed) compares to the local escape speed from the gravitationally bound system. A characteristic radius for thermal evaporation is the “gravitational radius” r_g , where the sound speed equals the escape speed:

$$r_g = \frac{GM_* \mu m_p}{kT} \sim 100 \text{ AU} \left(\frac{T}{1000 \text{ K}} \right)^{-1} \left(\frac{M_*}{M_\odot} \right). \quad (3)$$

Early analytic models made the simple assumption that photoevaporation occurred for $r > r_g$, and that the warm surface was gravitationally bound for $r < r_g$. However, a closer look at the gas dynamics shows that this division happens not at r_g but at about $0.1 - 0.2 r_g$ (Liffman, 2003; Adams *et al.*, 2004; Font *et al.*, 2004), and that this division is not entirely sharp. In other words, photoevaporation happens *mostly* outside of the “critical radius” $r_{\text{cr}} \sim 0.15 r_g$, though a weak evaporation occurs inside of r_{cr} . Since these are important new insights since PPIV, we devote a subsection on them below.

With $T \sim 10^4$ K the critical radius for EUV-induced photoevaporation is $r_{\text{cr}}(\text{EUV}) \sim 1 - 2(M_*/M_\odot)$ AU. However, there is no fixed $r_{\text{cr}}(\text{FUV})$ because the FUV-heated gas has temperatures that depend on FUV flux and gas density, i.e., on r and z . Therefore, $r_{\text{cr}}(\text{FUV})$ depends on r and z , and may range from 3-150 AU for solar mass stars.

The evaporative mass flux $\dot{\Sigma}$ depends not only on the temperature of the photon-heated gas, but also on the ver-

tical penetration depth of the FUV/EUV photons. For EUV photons this is roughly set for $r < r_{\text{cr}} \sim 1$ AU by the Strömgren condition that recombinations in the ionized layer equal the incident ionizing flux. Neglecting dust attenuation, this penetration column can be expressed: $A_V(\text{EUV}) \sim 0.05 \delta \Phi_{41}^{1/2} (r/\text{AU})^{-1/2}$, where $\Phi_{41} \equiv \Phi_{\text{EUV}}/10^{41}$ photons/s and δ is the ratio of the dust surface area per hydrogen to the interstellar dust value (see Section 4 and note that δ can be much smaller than unity if dust has settled or coagulated). Outside of 1 AU, the penetration depth falls even faster with r , roughly as $r^{-3/2}$ (see Hollenbach *et al.* 1994). On the other hand, the FUV penetration depth is set by dust attenuation, or $A_V(\text{FUV}) \sim \varphi$, where we recall that φ is the irradiation angle and depends on disk flaring. In general $A_V(\text{EUV}) \ll A_V(\text{FUV})$, so the EUV-ionized skin of the disk lies on top of the FUV-heated gas surface layer.

The penetration depth is an important quantity because it sets the density at the base of the photoevaporative flow: the deeper the penetration depth, the higher the density. The flux of outflowing matter is proportional to the product of local density and sound speed within this heated layer. This is why the complex surface structure models of Section 4 are so important for FUV-driven photoevaporation. For EUV-driven photoevaporation, on the other hand, the situation is less complicated, since the temperature in the ionized skin of the disk is independent of r and z , as long as $z > z_b$, where z_b is the bottom of the ionized layer, i.e. the base of the flow. For this simple case, the evaporative mass flux originates at z_b , which is where the highest density gas at temperature $T_{\text{EUV}} \simeq 10^4$ K resides.

Although FUV-heated layers have lower temperatures than the EUV-heated skin they are at higher densities and may equally well initiate the flow and determine the mass flux as EUV photons (see Johnstone *et al.*, 1998 for a similar situation for externally illuminated disks). Gorti and Hollenbach (in preparation, henceforth GH06) find that the FUV-photoevaporative flow typically originates at vertical heights where $T \sim 100 - 200$ K, yielding $r_{\text{cr}} \sim 50 - 100$ AU. For $r > 50$ AU, the FUV photoevaporation dominates. On the other hand, EUV photons (with $r_{\text{cr}} \sim 1$ AU) affect the planet forming regions at $r \ll 50$ AU more than the FUV photons.

5.2.2. Photoevaporation as a Bernoulli flow. One way to understand why the disk can evaporate at radii as small as $0.2 r_g$ is to consider the evaporative flow as a Bernoulli flow along streamlines (Liffman, 2003; Adams *et al.*, 2004). These streamlines initially rise nearly vertically out of the disk and then bend over to become asymptotically radially outward streamlines. If a streamline starts at $r > r_g$, then the flow rapidly goes through a sonic point and achieves the sound speed c_s near the base of the flow. The mass flux rate in the flow is then $\dot{\Sigma} \simeq \rho_b c_s$, where ρ_b is the mass density of the gas at the base.

On the other hand, if a streamline starts at $r \ll r_g$, the gas at its base lies deep in the gravitational potential.

As a simplification let us now treat these streamlines as if they are entirely radial streamlines (ignoring their vertical rise out of a disk). Then the standard atmospheric solution has a density that falls off from r to roughly r_g as $\exp(-r_g/2r)$. The gas flows subsonically and accelerates, as it slowly expands outward, until it passes through a sonic point at $r_s \lesssim 0.5r_g$ ($0.5r_g$ is the classic Parker wind solution for zero rotation). For $r \ll r_g$, the mass flux is reduced considerably by the rapid fall-off of the density from r to r_s . For $r < r_g$, the mass flux is roughly given by the density at r_s times the sound speed times the dilution factor $(r_s/r)^2$ that accounts for mass conservation between r and r_s : $\dot{\Sigma} \simeq \rho_b e^{-r_g/2r} c_s (r_s/r)^2$. Assuming the same ρ_b and c_s at all r , we see that $\dot{\Sigma}(0.2r_g) \simeq 0.5\dot{\Sigma}(r_g)$ and that $\dot{\Sigma}(0.1r_g) \simeq 0.17\dot{\Sigma}(r_g)$. This demonstrates that $r_{\text{cr}} \sim 0.15r_g$ for this simplified case, and that even for $r \lesssim r_{\text{cr}}$ evaporation is weak, but not zero. In Fig. 7 the base of the flow is marked with the large dot (though that figure shows a static, non-evaporating model with only FUV heating). In that figure, T_{virial} is the temperature such that the sound speed equals the escape speed; $T_{\text{evap,crit}} \equiv 0.2T_{\text{virial}}$ is roughly where the photoevaporation flow originates (i.e., where $r = r_{\text{cr}}$).

5.2.3. Mass loss rates for EUV-induced flows. Although central star FUV models are not yet published, several central star EUV models have appeared in the literature. *Hollenbach et al.* (1994) first outlined the essential physics of EUV-induced flows by the central star and presented an approximate analytic solution to the mass loss rate for a disk larger than r_g . The basic physics is the Strömgren relation, $\Phi_{\text{EUV}} \simeq \alpha_r n_e^2 r^3$, where α_r is the hydrogen recombination coefficient and n_e is the electron density in the ionized surface gas. This sets the hydrogen nucleus (proton) number density at the base of the flow $n_b \propto \Phi_{\text{EUV}}^{1/2}$, and therefore an identical proportionality for the mass loss rate:

$$\dot{M}_{\text{EUV}} \sim 4 \times 10^{-10} \left(\frac{\Phi_{\text{EUV}}}{10^{41} \text{ s}^{-1}} \right)^{0.5} \left(\frac{M_\star}{M_\odot} \right)^{0.5} \quad (4)$$

in units of M_\odot/yr . Radiation hydrodynamical simulations (*Yorke and Welz*, 1996; *Richling and Yorke*, 1997) find a similar power-law index for the dependence of the mass-loss rate on the EUV photon rate of the central star. This result applies for both high and low mass central stars, and is valid for a weak stellar wind. The effect of a strong stellar wind is such that the ram pressure reduces the scale height of the atmosphere above the disk and the EUV photons are allowed to penetrate more easily to larger radii. This increases the mass-loss rate from the outer parts of the disk. It is noteworthy that the diffuse EUV field, caused by recombining electrons and protons in the disk's ionized atmosphere inside r_{cr} , controls the EUV-induced mass-loss rates (*Hollenbach et al.*, 1994) for disks with no or small inner holes ($< r_{\text{cr}}$). This effect negates any potential for self-shadowing of the EUV by the disk.

5.3. Evolution of photoevaporating disks

5.3.1. Case without viscous evolution. Let us first assume a disk that does not viscously evolve: it just passively undergoes photoevaporation. For disks with size $r_d < r_{\text{cr}}$, the photoevaporation proceeds from outside in. The mass flux rate at r_d is much higher than inside of r_d , because the gas at r_d is least bound. In addition, disk surface densities generally fall with r (see Section 2). Therefore, the disk shrinks as it photoevaporates, and most of the mass flux comes from the outer disk radius. However, for disks with $r_d > r_{\text{cr}}$, two types of disk evolution may occur. For EUV photons, *Hollenbach et al.* (1994) showed that the mass flux $\dot{\Sigma}$ beyond r_{cr} goes roughly as $r^{-2.5}$ if there is no inner hole extending to r_{cr} . The timescale for complete evaporation at r goes as $\Sigma(r)/\dot{\Sigma}(r)$. As long as Σ does not drop faster than $r^{-2.5}$, the disk will evaporate first at $r \sim r_{\text{cr}}$, and, once a gap forms there, will then steadily erode the disk from this gap outwards.

If, on the other hand, $\Sigma(r)/\dot{\Sigma}(r)$ decreases with r , then the disk shrinks from outside in as in the $r_d < r_{\text{cr}}$ case. The photoevaporation by the FUV from the central star has not yet been fully explored, but preliminary work by GH06 suggests that the mass flux $\dot{\Sigma}$ in the outer disks around solar mass stars *increases* with r . In this case, the disk evaporates from outside in for most generally assumed surface density laws, which decrease with r . The combined effect of EUV and FUV photoevaporation then is likely to erode the disk outwards from $r_{\text{cr}}(\text{EUV}) \sim 1$ AU by the EUV flow and inwards from the outer disk radius by the FUV flow, sandwiching the intermediate radii.

5.3.2. Case with viscous evolution. Now let us consider a disk that is actively accreting onto the star (see Section 2). In general, if the photoevaporation drills a hole somewhere in the disk or ‘eats’ its way from outside in, the forces of viscous spreading tend to move matter toward these photoevaporation regions, which can accelerate the dissipation of the disk. If the disk has a steady accretion rate \dot{M} , then a gap forms once $\dot{M}_{\text{evap}} \propto r^2 \dot{\Sigma}$ exceeds \dot{M} . Since $r^2 \dot{\Sigma} \propto r^{-0.5}$ for EUV photoevaporation beyond r_{cr} , the gap first forms at the minimum radius ($\sim r_{\text{cr}}$) and then works its way outward. *Clarke et al.* (2001) presented time-dependent computations of the evolution of disks around low mass stars with $\Phi_{\text{EUV}} \sim 10^{41-43}$ photons s^{-1} . Their model combines EUV photoevaporation with a viscous evolution code. However, they used the current hypothesis at that time that evaporation only occurs outside of r_g . After $\sim 10^6$ to 10^7 years of viscous evolution relatively unperturbed by photoevaporation, the viscous accretion inflow rates fall below the photoevaporation rates at r_g . At this point, a gap opens up at r_g and the inner disk rapidly (on an inner disk viscous timescale of $\sim 10^5$ yr) drains onto the central star or spreads to r_g where it evaporates. In this fashion, an inner hole is rapidly produced extending to r_g .

Alexander et al. (2006a, 2006b) extended the work of *Clarke et al.* to include the effect of $r_{\text{cr}} < r_g$, and to treat

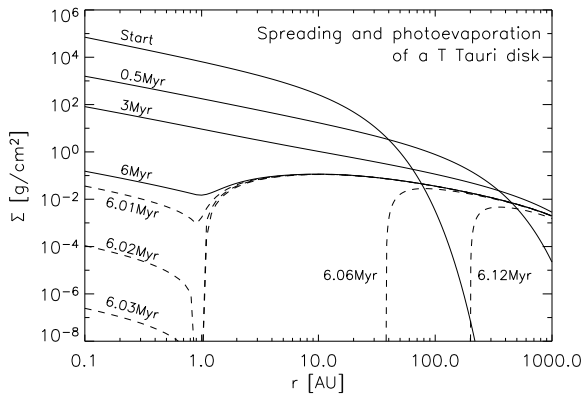


Fig. 11.— Evolution of the surface density of a EUV-photoevaporating disk (Figure adapted from *Alexander et al.*, 2006b). This simulation starts from a given disk structure of about $0.05 M_{\odot}$ (marked with ‘Start’ in the figure). Initially the disk accretes and viscously spreads (solid lines). At $t = 6 \times 10^6$ yr the photoevaporation starts affecting the disk. Once the EUV-photoevaporation has drilled a gap in the disk at ~ 1 AU, the destruction of the disk goes very rapidly (dashed lines). The inner disk quickly accretes onto the star, followed by a rapid erosion of the outer disk from inside out. In this model the disk viscosity spreads to > 1000 AU; however, FUV-photoevaporation (not included) will likely truncate the outer disk.

the outward EUV evaporation of the disk beyond $r_{\text{cr}} \sim 1$ AU. They show that once the inner hole is produced, the diffuse flux from the atmosphere of the inner disk is removed and the attenuation of the direct flux by this same atmosphere is also removed. This enhances the EUV photoevaporation rate by the direct EUV flux from the star, and the effect magnifies as the inner hole grows as $\dot{M}_{\text{EUV}} \propto r_{\text{inner}}^{1/2}$, again derivable from a simple Strömgren criterion. The conclusion is that the outer disk is very rapidly cleared once the inner hole forms (see Fig. 11).

The rapid formation of a cleared out inner hole almost instantly changes the nature and appearance of the disk. The above authors compare their model favorably with a number of observations: (i) the rapid transition from classical T Tauri stars to weak line T Tauri stars, (ii) the almost simultaneous loss of the outer disk (as detected by submillimeter measurements of the dust continuum) with the inner disk (as detected by near IR observations of very hot dust near the star), and (iii) the SED observations of large (3–10 AU) inner holes in those sources (see dotted line of Fig. 5) with evidence for low accretion rates and intermediate mass outer disks such as the source CoKu Tau/4. Fig. 12 shows the evolutionary tracks of their models with $\Phi_{\text{EUV}} = 10^{42}$ photons/s compared to the observations of weak-line T Tauri stars (WTTs) and CTTSs.

In a similar vein *Armitage et al.* (2003) used the combination of EUV photoevaporation and viscous dispersal,

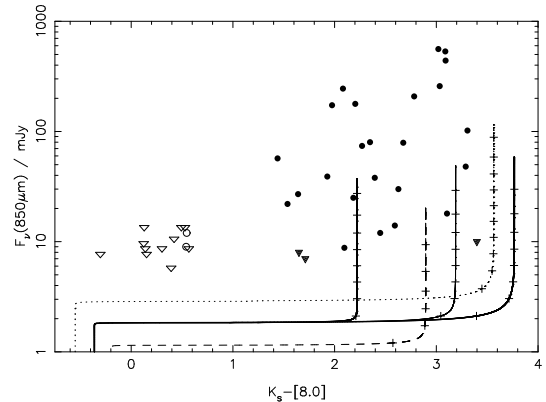


Fig. 12.— Near- to mid-infrared color (in magnitudes) versus $850 \mu\text{m}$ flux for photoevaporation/viscous evolution models. The data are taken from *Hartmann et al.* (2005) and *Andrews and Williams* (2005): $850 \mu\text{m}$ detections (circles) and upper limits (triangles) are plotted for both CTTSs (filled symbols) and WTTs (open symbols). Evolutionary tracks are shown for models with stellar masses 0.5 (dashed), 1.0 (solid), and $2.0 M_{\odot}$ (dotted), at a disk inclination of $i = 60^{\circ}$ to the line of sight. The thick tracks to the right and left show the $1 M_{\odot}$ model at $i = 0$ and $i = 80^{\circ}$, respectively. Crosses are added every 1 Myr to show the temporal evolution. Initially the (optically thin) $850 \mu\text{m}$ flux declines slowly at constant (optically thick) infrared color. However, once the viscous accretion rate falls below the photoevaporation rate, the disk is rapidly cleared from the inside-out. (Figure adapted from *Alexander et al.* 2006b.)

together with an assumed dispersion of a factor of 3 in the initial disk mass, to explain the dispersion in the lifetime and accretion rates of T Tauri disks. They found that the models predict a low fraction of binaries that pair a classical T Tauri star with a weak-lined T Tauri star. Their models are in better agreement with observations of disk lifetimes in binaries than models without photoevaporation.

Going one step further, *Takeuchi et al.* (2005) constructed models combining viscous evolution, EUV photoevaporation, and the differential radial motion of grains and gas. Their models predicted that for low-mass stars with a low photoevaporation rate, dust-poor gas disks with an inner hole would form (WTTs), whereas for high mass stars (evolved Herbig Ae/Be) with a high photoevaporation rate, gas-poor dust rings would form.

Matsuyama et al. (2003) pointed out that if the EUV luminosity is created by accretion onto the star, then, as the accretion rate diminishes, the EUV luminosity drops and the timescale to create a gap greatly increases. Even worse, as discussed above, the EUV photons are unlikely to escape the accretion column. Only if the EUV luminosity remains high due to chromospheric activity does EUV photoevaporation play an important role in the evolution of disks around isolated low mass stars. *Alexander et al.* (2005)

argue this is the case. *Ruden* (2004) provides a detailed analytic analysis which describes the evolution of disks in the presence of viscous accretion and photoevaporation and compares his results favorably with these two groups.

5.4. Effect on planet formation

The processes which disperse the gas influence the formation of planets. Small dust particles follow the gas flow. If the gas is dispersed before the dust can grow, all the dust will be lost in the gas dispersal and planetesimals and planets will not form. Even if there is time for particles to coagulate and build sufficiently large rocky cores that can accrete gas (*Pollack et al.*, 1996; *Hubickyj et al.*, 2004), the formation of gas giant planets like Jupiter and Saturn will be suppressed if the gas is dispersed before the accretion can occur. Furthermore, gas dispersal helps trigger gravitational instabilities that may lead to planetesimal formation (*Goldreich and Ward*, 1973; *Youdin and Shu*, 2002; *Throop et al.*, 2005), affects planet migration (e.g., *Ward*, 1997) and influences the orbital parameters of planetesimals and planets (*Kominami and Ida*, 2002).

5.4.1. Gas Rich Versus Gas Poor Giant Planets in the Solar System. *Shu et al.* (1993) showed that with $\Phi_{\text{EUV}} \sim 10^{41}$ photons s^{-1} , the early Sun could have photoevaporated the gas beyond Saturn before the cores of Neptune and Uranus formed, leaving them gas poor. However, this model ignored photoevaporation inside of r_g . The current work by *Adams et al.* (2004) would suggest rather rapid photoevaporation inside of 10 AU, and make the timing of this scenario less plausible. FUV photoevaporation (either from external sources or from the central star) may provide a better explanation. Preliminary results from GH06 suggest that the early Sun did not produce enough FUV generally to rapidly remove the gas in the outer giant planet regions. *Adams et al.* and *Hollenbach and Adams*, (2005) discuss the external illumination case, which looks more plausible.

5.4.2. Truncation of the Kuiper Belt. A number of observations point to the truncation of Kuiper Belt Objects (KBOs) beyond about 50 AU (e.g., *Allen, Bernstein, and Malhotra*, 2002; *Trujillo and Brown*, 2001). *Adams et al.* (2004) and *Hollenbach and Adams* (2004, 2005) show that photoevaporation by a nearby massive star could cause truncation of KBOs at about 100 AU, but probably not 50 AU. The truncation is caused by the gas dispersal before the dust can coagulate to sizes which survive the gas dispersal, and which can then later form KBOs. Models of FUV photoevaporation by the early Sun are needed.

5.4.3. Formation of Planetesimals. In young disks, dust settles toward the midplane under the influence of the stellar gravity and coagulates. Once coagulated dust has concentrated in the midplane, the roughly centimeter-sized particles can grow further by collisions or by local gravitational instability (*Goldreich and Ward*, 1973; *Youdin and Shu*,

2002). A numerical model by *Throop and Bally* (2005) follows the evolution of gas and dust independently and considers the effects of vertical sedimentation and external photoevaporation. The surface layer of the disk becomes dust-depleted which leads to dust-depleted evaporating flows. Because of the combined effects of the dust settling and the gas evaporating, the dust-to-gas ratio in the disk midplane is so high that it meets the gravitational instability criteria of *Youdin and Shu* (2002), indicating that kilometer-sized planetesimals could spontaneously form. These results imply that photoevaporation may even trigger the formation of planetesimals. Presumably, photoevaporation by the central star may also produce this effect.

6. SUMMARY AND OUTLOOK

In this chapter we have given a brief outline of how disks form and viscously evolve, what their structure is, what their spectra look like in dust continuum and in gas lines, and how they might come to their end by photoevaporation and viscous dispersion. The disk structure in dust and gas is summarized in Fig. 13. Evidently, due to the broadness of the topic we had to omit many important issues. For instance the formation of disks is presumably much more chaotic than the simple picture we have discussed. In recent years there is a trend to outfit even the observation-oriented workhorse models with ever more detailed physics. This is not a luxury, since the volume of observational data (both spectral and spatial) is increasing dramatically, as shown by various other chapters in this book. For instance, with observational information about dust growth and sedimentation in disks, it will be necessary to include realistic dust evolution models into the disk models. Additionally, with clear evidence for non-axial symmetry in many disks (e.g., *Fukagawa et al.*, 2004) modelers may be forced to abandon the assumption of axial symmetry. The thermal-chemical study of the gas in the disk surface layers is a rather new field, and more major developments are expected in the next few years, both in theory and in the comparison to observations. These new insights will also influence the models of FUV-photoevaporation, and thereby the expected disk lifetime.

A crucial step to aim for in the future is the unification of the various aspects discussed here. They are all intimately connected together and mutually influence each other. Such a unification opens up the perspective of connecting seemingly unrelated observations and thereby improving our understanding of the bigger picture.

Acknowledgments: The authors would like to thank Al Glassgold, Malcolm Walmsley, Klaus Pontoppidan and Jes Joergensen for proof-reading and providing very useful comments.

REFERENCES

Acke B. and van den Ancker M. E. (2006) *astro-ph/0512562*.

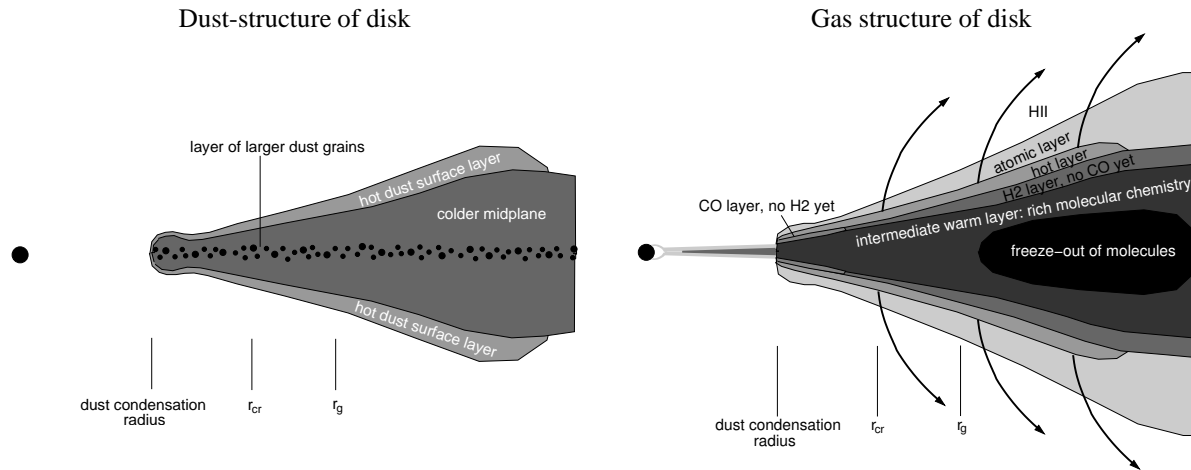


Fig. 13.— Pictograms of the structure of a flaring protoplanetary disk, in dust (left) and gas (right).

- Acke B., van den Ancker M. E., and Dullemond C. P. (2005) *Astron. Astrophys.*, 436, 209–230.
- Acke B., van den Ancker M. E., Dullemond C. P., van Boekel R., and Waters L. B. F. M. (2004) *Astron. Astrophys.*, 422, 621–626.
- Adams F. C., Hollenbach D., Laughlin G., and Gorti U. (2004) *Astrophys. J.*, 611, 360–379.
- Adams F. C. and Shu F. H. (1986) *Astrophys. J.*, 308, 836–853.
- Aikawa Y. and Herbst E. (1999) *Astron. Astrophys.*, 351, 233–246.
- Aikawa Y., van Zadelhoff G. J., van Dishoeck E. F., and Herbst E. (2002) *Astron. Astrophys.*, 386, 622–632.
- Akeson R. L., Walker C. H., Wood K., Eisner J. A., Scire E., Penprase B., Ciardi D. R., van Belle G. T., Whitney B., and Bjorkman J. E. (2005) *Astrophys. J.*, 622, 440–450.
- Alexander R. D., Clarke C. J., and Pringle J. E. (2004a) *Mon. Not. R. Astron. Soc.*, 348, 879–884.
- Alexander R. D., Clarke C. J., and Pringle J. E. (2004b) *Mon. Not. R. Astron. Soc.*, 354, 71–80.
- Alexander R. D., Clarke C. J., and Pringle J. E. (2005) *Mon. Not. R. Astron. Soc.*, 358, 283–290.
- Alexander R. D., Clarke C. J., and Pringle J. E. (2006a) *Mon. Not. R. Astron. Soc. in press*.
- Alexander R. D., Clarke C. J., and Pringle J. E. (2006b) *Mon. Not. R. Astron. Soc. in press*.
- Allen R. L., Bernstein G. M., and Malhotra R. (2002) *Astron. J.*, 124, 2949–2954.
- Andrews, S. M. and Williams, J. P. (2005) *Astrophys. J.*, 631, 1134–1160.
- Armitage P. J., Livio M., and Pringle J. E. (2001) *Mon. Not. R. Astron. Soc.*, 324, 705–711.
- Armitage P. J., Clarke C. J., and Palla F. (2003) *Mon. Not. R. Astron. Soc.*, 342, 1139–1146.
- Artymowicz P. and Lubow S. H. (1994) *Astrophys. J.*, 421, 651–667.
- Balbus S. and Hawley J. (1991) *Astrophys. J.*, 376, 214–233.
- Bary J. S., Weintraub D. A., and Kastner J. H. (2003) *Astrophys. J.*, 586, 1136–1147.
- Bell K. R. and Lin D. N. C. (1994) *Astrophys. J.*, 427, 987–1004.
- Bell K. R., Cassen P. M., Klahr H. H., and Henning T. (1997) *Astrophys. J.*, 486, 372–387.
- Bell K. R. (1999) *Astrophys. J.*, 526, 411–434.
- Bergin E., Calvet N., D’Alessio P., and Herczeg G. J. (2003) *Astrophys. J.*, 591, L159–L162.
- Bertout C., Basri G., and Bouvier J. (1988) *Astrophys. J.*, 330, 350–373.
- Bjorkman J. E. and Wood K. (2001) *Astrophys. J.*, 554, 615–623.
- Blandford R. D. and Payne D. G. (1982) *Mon. Not. R. Astron. Soc.*, 199, 883–903.
- Bonnell I. and Bastien P. (1992) *Astrophys. J.*, 401, L31–L34.
- Boss A. P. (1996) *Astrophys. J.*, 469, 906–920.
- Boss A. P. (1997) *Astrophys. J.*, 478, 828–828.
- Bouwman J., de Koter A., Dominik C., and Waters L. B. F. M. (2003) *Astron. Astrophys.*, 401, 577–592.
- Brittain S. D., Rettig T. W., Simon T., Kulesa C., DiSanti M. A., and Dello Russo N. (2003) *Astrophys. J.*, 588, 535–544.
- Calvet N., D’Alessio P., Hartmann L., Wilner D., Walsh A., and Sitko M. (2002) *Astrophys. J.*, 568, 1008–1016.
- Calvet N., Hartmann L., and Strom S. E. (2000) *Protostars and Planets IV*, Proceedings of the Conference held in Santa Barbara, July 1998, Eds. V. Mannings, A. P. Boss and S. S. Russell, pp. 377–399.
- Calvet N., Patino A., Magris G. C., and D’Alessio P. (1991) *Astrophys. J.*, 380, 617–630.
- Carpenter J. M., Wolf S., Schreyer K., Launhardt R., and Henning T. (2005) *Astron. J.*, 129, 1049–1062.
- Cassen P. (1996) *Meteoritics and Planetary Science*, 31, 793–806.
- Chiang E. I. and Goldreich P. (1997) *Astrophys. J.*, 490, 368–376. [CG97]
- Chiang E. I., Joung M. K., Creech-Eakman M. J., Qi C., Kessler J. E., Blake G. A., and van Dishoeck E. F. (2001) *Astrophys. J.*, 547, 1077–1089.
- Clarke C. J., Gendrin A., and Sotomayor M. (2001) *Mon. Not. R. Astron. Soc.*, 328, 485–491.
- Clarke C. J. and Syer D. (1996) *Mon. Not. R. Astron. Soc.*, 278, L23–L27.
- D’Alessio P., Calvet N., and Hartmann L. (2001) *Astrophys. J.*,

- 553, 321–334.
- D'Alessio P., Calvet N., Hartmann L., Franco-Hernández R., and Servín H. (2006) *Astrophys. J.*, 638, 314–335.
- D'Alessio P., Calvet N., Hartmann L., Lizano S., and Cantó J. (1999) *Astrophys. J.*, 527, 893–909.
- D'Alessio P., Canto J., Calvet N., and Lizano S. (1998) *Astrophys. J.*, 500, 411–427.
- D'Alessio P., Hartmann L., Calvet N., Franco-Hernández R., Forrest W. J., Sargent B. et al. (2005) *Astrophys. J.*, 621, 461–472.
- Dent W. R. F., Greaves J. S., and Coulson I. M. (2005) *Mon. Not. R. Astron. Soc.*, 359, 663–676.
- Dominik C., Dullemond C. P., Waters L. B. F. M., and Walch S. (2003) *Astron. Astrophys.*, 398, 607–619.
- Dubrulle B., Marié L., Normand C., Richard D., Hersant F., and Zahn J.-P. (2005) *Astron. Astrophys.*, 429, 1–13.
- Dullemond C. P. (2002) *Astron. Astrophys.*, 395, 853–862. [D02]
- Dullemond C. P. and Dominik C. (2004a) *Astron. Astrophys.*, 417, 159–168. [DD04a]
- Dullemond C. P. and Dominik C. (2004b) *Astron. Astrophys.*, 421, 1075–1086. [DD04b]
- Dullemond C. P., Dominik C., and Natta A. (2001) *Astrophys. J.*, 560, 957–969. [DDN01]
- Dullemond C. P., van den Ancker M. E., Acke B., and van Boekel R. (2003) *Astrophys. J.*, 594, L47–L50.
- Dullemond C. P., van Zadelhoff G. J., and Natta A. (2002) *Astron. Astrophys.*, 389, 464–474.
- Eisner J. A., Lane B. F., Akeson R. L., Hillenbrand L. A., and Sargent A. I. (2003) *Astrophys. J.*, 588, 360–372.
- Font A. S., McCarthy I. G., Johnstone D., and Ballantyne D. R. (2004) *Astrophys. J.*, 607, 890–903.
- Forrest W. J., Sargent B., Furlan E., D'Alessio P., Calvet N., Hartmann L. et al. (2004) *Astrophys. J. Suppl.*, 154, 443–447.
- Friedjung M. (1985) *Astron. Astrophys.*, 146, 366–368.
- Fromang S., Balbus S. A., and De Villiers J.-P. (2004) *Astrophys. J.*, 616, 357–363.
- Fukagawa M., Hayashi M., Tamura M., Itoh Y., Hayashi S. S., and Oasa Y. e. a. (2004) *Astrophys. J.*, 605, L53–L56.
- Gammie C. F. (1996) *Astrophys. J.*, 457, 355–362.
- Gammie C. F. and Johnson B. M. (2005) in *ASP Conf. Ser. 341: Chondrites and the Protoplanetary Disk*, pp. 145–164.
- Glassgold A. E., Najita J., and Igea J. (1997a) *Astrophys. J.*, 480, 344–350.
- Glassgold A. E., Najita J., and Igea J. (1997b) *Astrophys. J.*, 485, 920–920.
- Goldreich P. and Ward W. R. (1973) *Astrophys. J.*, 183, 1051–1062.
- Gorti U. and Hollenbach D. (2004) *Astrophys. J.*, 613, 424–447.
- Habing H. J. (1968) *Bull. Astron. Inst. Netherlands*, 19, 421–431.
- Haisch K. E., Lada E. A., and Lada C. J. (2001) *Astrophys. J.*, 553, L153–L156.
- Hartmann L., Calvet N., Gullbring E., and D'Alessio P. (1998) *Astrophys. J.*, 495, 385–400.
- Hartmann L., Megeath S. T., Allen L., Luhman K., Calvet N., D'Alessio P., Franco-Hernandez R. and Fazio G. (2005) *Astrophys. J.*, 629, 881–896
- Hayashi C. (1981) in *IAU Symp. 93: Fundamental Problems in the Theory of Stellar Evolution*, pp. 113–126.
- Hillenbrand L. A., Strom S. E., Vrba F. J., and Keene J. (1992) *Astrophys. J.*, 397, 613–643.
- Hollenbach D. and Adams F. (2005) in *Star Formation in the Interstellar Medium* (D. Lin, D. Johnstone, F. Adams, D. Neufeld, and E. Ostriker, eds.), ASP Conference Series, pp. 3, Provo: Pub. Astr. Soc. Pacific.
- Hollenbach D. and Adams F. C. (2004) in *ASP Conf. Ser. 324: Debris Disks and the Formation of Planets*, pp. 168–183.
- Hollenbach D., Gorti U., Meyer M., Kim J. S., Morris P., Najita J. et al. (2005) *Astrophys. J.*, 631, 1180–1190.
- Hollenbach D., Johnstone D., Lizano S., and Shu F. (1994) *Astrophys. J.*, 428, 654–669.
- Hollenbach D. J., Yorke H. W., and Johnstone D. (2000) *Protostars and Planets IV*, Proceedings of the Conference held in Santa Barbara, July 1998, Eds. V. Mannings, A. P. Boss and S. S. Russell, pp. 401–428.
- Hubickyj O., Bodenheimer P., and Lissauer J. J. (2004) in *rev. Mex. Astron. Astrofis. Conf. ser.*, pp. 83–86.
- Hueso R. and Guillot T. (2005) *Astron. Astrophys.*, 442, 703–725. [HG05]
- Ilgner M. and Nelson R. P. (2006) *Astron. Astrophys.*, 445, 205–222.
- Isella A. and Natta A. (2005) *Astron. Astrophys.*, 438, 899–907.
- Jin L. (1996) *Astrophys. J.*, 457, 798–804.
- Johnstone D., Hollenbach D., and Bally J. (1998) *Astrophys. J.*, 499, 758–776.
- Jonkheid B., Faas F. G. A., van Zadelhoff G.-J., and van Dishoeck E. F. (2004) *Astron. Astrophys.*, 428, 511–521.
- Jonkheid B., Kamp I., Augereau J.-C., and van Dishoeck E.F. (2006) *Astron. Astrophys. submitted*
- Kamp I. and Bertoldi F. (2000) *Astron. Astrophys.*, 353, 276–286.
- Kamp I. and van Zadelhoff G.-J. (2001) *Astron. Astrophys.*, 373, 641–656.
- Kamp I., van Zadelhoff G.-J., van Dishoeck E. F., and Stark R. (2003) *Astron. Astrophys.*, 397, 1129–1141.
- Kamp I. and Dullemond C. P. (2004) *Astrophys. J.*, 615, 991–999.
- Kamp I., Dullemond C. P., Hogerheijde M., and Emilio Enriquez J. (2006) *Proceedings IAU Symp. Nr. 231: Astrochemistry – Recent Successes and Current Challenges*. Eds. D.C. Lis, G.A. Blake and E. Herbst.
- Kawazoe E. and Mineshige S. (1993) *PASJ*, 45, 715–725.
- Kenyon S. J. and Hartmann L. (1987) *Astrophys. J.*, 323, 714–733.
- Kenyon S. J. and Hartmann L. (1991) *Astrophys. J.*, 383, 664–673.
- Kenyon S. J. and Hartmann L. (1995) *Astrophys. J. Suppl.*, 101, 117–171.
- Kessler-Silacci J., Augereau J.-C., Dullemond C., Geers V., Lahuis F. et al. (2006) *Astrophys. J.*, 639, 275–291.
- Kitamura Y., Momose M., Yokogawa S., Kawabe R., Tamura M., and Ida S. (2002) *Astrophys. J.*, 581, 357–380.
- Klahr H. H. and Bodenheimer P. (2003) *Astrophys. J.*, 582, 869–892.
- Kominami J. and Ida S. (2002) *Icarus*, 157, 43–56.
- Lachaume R., Malbet F., and Monin J.-L. (2003) *Astron. Astrophys.*, 400, 185–202.
- Lachaume R. (2004) *Astron. Astrophys.*, 422, 171–176.
- Laughlin G. and Bodenheimer P. (1994) *Astrophys. J.*, 436, 335–354.
- Liffman K. (2003) *Pub. Astron. Soc. Australia*, 20, 337–339.
- Lissauer J. J. (1993) *Annu. Rev. Astron. Astrophys.*, 31, 129–174.
- Lucy L. B. (1999) *Astron. Astrophys.*, 344, 282–288.
- Lynden-Bell D. (1969) *Nature*, 223, 690–694.
- Lynden-Bell D. and Pringle J. E. (1974) *Mon. Not. R. Astron. Soc.*, 168, 603–637.
- Malbet F. and Bertout C. (1991) *Astrophys. J.*, 383, 814–819.
- Matsumoto T. and Hanawa T. (2003) *Astrophys. J.*, 595, 913–934.
- Matsuyama I., Johnstone D., and Hartmann L. (2003) *Astrophys. J.*, 582, 893–904.

- Meeus G., Waters L. B. F. M., Bouwman J., van den Ancker M. E., Waelkens C., and Malfait K. (2001) *Astron. Astrophys.*, 365, 476–490. [M01]
- Meyer M. R., Hillenbrand L. A., Backman D. E., Beckwith S. V. W., Bouwman J. et. al. (2004) *Astrophys. J. Suppl.*, 154, 422–427.
- Miyake K. and Nakagawa Y. (1995) *Astrophys. J.*, 441, 361–384.
- Monnier J. D., Millan-Gabet R., Billmeier R., Akeson, R. L., Wallace, D. et. al. (2005) *Astrophys. J.*, 624, 832–840.
- Muzerolle J., Hillenbrand L., Calvet N., Briceño C. and Hartmann L. (2003a) *Astrophys. J.*, 592, 266–281.
- Muzerolle J., Calvet N., Hartmann L., and D’Alessio P. (2003b) *Astrophys. J.*, 597, L149–L152.
- Muzerolle J., D’Alessio P., Calvet N., and Hartmann L. (2004) *Astrophys. J.*, 617, 406–417.
- Muzerolle J., Luhman K. L., Briceño C., Hartmann L., and Calvet N. (2005) *Astrophys. J.*, 625, 906–912.
- Nakamoto T. and Nakagawa Y. (1994) *Astrophys. J.*, 421, 640–650. [NN94]
- Natta A., Prusti T., Neri R., Wooden D., Grinin V. P., and Mannings V. (2001) *Astron. Astrophys.*, 371, 186–197.
- Natta A., Testi L., Muzerolle J., Randich S., Comerón F., and Persi P. (2004) *Astron. Astrophys.*, 424, 603–612.
- Niccolini G., Woitke P., and Lopez B. (2003) *Astron. Astrophys.*, 399, 703–716.
- Nomura H. (2002) *Astrophys. J.*, 567, 587–595.
- Nomura H. and Millar T. J. (2005) *Astron. Astrophys.*, 438, 923–938.
- Pascucci I., Meyer M., Gorti U., Hollenbach D., Hillenbrand L., Carpenter J. et al. (2005) in *Protostars and Planets V, LPI Contribution No. 1286.*, #8468.
- Pfalzner S., Umbreit S., and Henning T. (2005) *Astrophys. J.*, 629, 526.
- Pickett B. K., Mejía A. C., Durisen R. H., Cassen P. M., Berry D. K., and Link R. P. (2003) *Astrophys. J.*, 590, 1060–1080.
- Pollack J. B., Hubickyj O., Bodenheimer P., Lissauer J. J., Podolak M., and Greenzweig Y. (1996) *Icarus*, 124, 62–85.
- Reyes-Ruiz M. and Stepinski T. F. (1996) *Astrophys. J.*, 459, 653–665.
- Richling S., Hollenbach D., and Yorke H. (2006) in *Planet Formation* (H. Klahr and W. Brandner, eds.), *Astrobiology*, pp. 38, Cambridge University Press.
- Richling S. and Yorke H. W. (1997) *Astron. Astrophys.*, 327, 317–324.
- Richter M. J., Jaffe D. T., Blake G. A., and Lacy J. H. (2002) *Astrophys. J.*, 572, L161–L164.
- Rucinski S. M. (1985) *Astron. J.*, 90, 2321–2330.
- Ruden S. P. (2004) *Astrophys. J.*, 605, 880–891.
- Ruden S. P. and Pollack J. B. (1991) *Astrophys. J.*, 375, 740–760.
- Sano T., Miyama S. M., Umebayashi T., and Nakano T. (2000) *Astrophys. J.*, 543, 486–501.
- Scally A. and Clarke C. (2001) *Mon. Not. R. Astron. Soc.*, 325, 449–456.
- Semenov D., Wiebe D., and Henning T. (2004) *Astron. Astrophys.*, 417, 93–106.
- Shakura N. I. and Sunyaev R. A. (1973) *Astron. Astrophys.*, 24, 337–355.
- Shu F. H., Johnstone D., and Hollenbach D. (1993) *Icarus*, 106, 92–101.
- Spaans M., Tielens A. G. G. M., van Dishoeck E. F., and Bakes E. L. O. (1994) *Astrophys. J.*, 437, 270–280.
- Stehle R. and Spruit H. C. (2001) *Mon. Not. R. Astron. Soc.*, 323, 587–600.
- Steinacker J., Henning T., Bacmann A., and Semenov D. (2003) *Astron. Astrophys.*, 401, 405–418.
- Stepinski T. F. (1998) *Astrophys. J.*, 507, 361–370.
- Stone J. M. and Pringle J. E. (2001) *Mon. Not. R. Astron. Soc.*, 322, 461–472.
- Störzer H. and Hollenbach D. (1999) *Astrophys. J.*, 515, 669–684.
- Takeuchi T., Clarke C. J., and Lin D. N. C. (2005) *Astrophys. J.*, 627, 286–292.
- Terebey S., Shu F. H., and Cassen P. (1984) *Astrophys. J.*, 286, 529–551.
- Thi W. F., van Dishoeck E. F., Blake G. A., van Zadelhoff G. J., Horn J., Becklin E. E., Mannings V., Sargent A. I., van den Ancker M. E., Natta A., and Kessler J. (2001) *Astrophys. J.*, 561, 1074–1094.
- Throop H. B. and Bally J. (2005) *Astrophys. J.*, 623, L149–L152.
- Tielens A. G. G. M. and Hollenbach D. (1985) *Astrophys. J.*, 291, 722–754.
- Tohline J. E. and Hachisu I. (1990) *Astrophys. J.*, 361, 394–407.
- Trujillo C. A. and Brown M. E. (2001) *Astrophys. J.*, 554, L95–L98.
- Tuthill P. G., Monnier J. D., and Danchi W. C. (2001) *Nature*, 409, 1012–1014.
- Vinković D., Ivezić Ž., Miroshnichenko A. S., and Elitzur M. (2003) *Mon. Not. R. Astron. Soc.*, 346, 1151–1161.
- Walker C., Wood K., Lada C. J., Robitaille T., Bjorkman J. E., and Whitney B. (2004) *Mon. Not. R. Astron. Soc.*, 351, 607–616.
- Ward W. R. (1997) *Icarus*, 126, 261–281.
- Wardle M. (2004) *Astrophys. Space Sci.*, 292, 317–323.
- Weidenschilling S. J. (1977) *Astrophys. Space Sci.*, 51, 153–158.
- Whitney B. A. and Hartmann L. (1992) *Astrophys. J.*, 395, 529–539.
- Willacy K. and Langer W. D. (2000) *Astrophys. J.*, 544, 903–920.
- Wilner D. J., Ho P. T. P., Kastner J. H., and Rodríguez L. F. (2000) *Astrophys. J.*, 534, L101–L104.
- Wolf S., Henning T., and Stecklum B. (1999) *Astron. Astrophys.*, 349, 839–850.
- Yamashita T., Handa T., Omodaka T., Kitamura Y., Kawazoe E., Hayashi S. S., and Kaifu N. (1993) *Astrophys. J.*, 402, L65–L67.
- Yorke H. W. and Bodenheimer P. (1999) *Astrophys. J.*, 525, 330–342.
- Yorke H. W., Bodenheimer P., and Laughlin G. (1993) *Astrophys. J.*, 411, 274–284.
- Youdin A. N. and Shu F. H. (2002) *Astrophys. J.*, 580, 494–505.
- Yorke H. W. and Welz A. (1996) *Astron. Astrophys.*, 315, 555–564.